Development and optimization of orally and topically applied liquid crystal-drug formulations

2017

Wesam R. Kadhum

Contents

Abbreviations

LC	liquid crystal
PABA	*p*-amino benzoic acid
MGE	C_{17}-monoglycerol ester
GMO	glycerol monoolate
TXA	tranexamic acid
4-MS	4-methoxy- salicylic acid
CC	catechin
Cal	calcein
SAXS	small-angle X-ray scattering
Lα	lamellar phase
V_2	cubic phase
H_2	hexagonal phase
GI	gastrointestinal
PHT	phytantriol
ERT	C_{22}-erythritol ester
a	lattice parameter
PBS	phosphate-buffered saline
i.v.	intravenous
p.o.	per oral
i.p.	intraperitoneal
AUC	the area under the plasma concentration-time curve
Im3m	primitive type (body-centered lattice)
Pn3m	diamond type (primitive lattice)
Ia3d	gyroid type (body-centered lattice)

Abstract

Liquid crystals (LCs) are semisolids made of lipids with crystalline structures combining the properties of both crystal and liquid states. First, the oral administration of LC formulations was evaluated. I aimed to develop oral formulations for delivering the drug to skin tissue with a high bioavailability using four different types of LC forming lipids (glyceryl monooleate (GMO), phytantriol (PHT), C_{17}-monoglycerol ester (MGE) and C_{22}-erythritol ester (ERT)) containing a mal-absorptive model compound, *p*-amino benzoic acid (PABA), which is an active element in cosmeceuticals, dietary supplements and skin disorder medicines. The bioavailability and skin concentration of PABA were investigated after its oral administration in rats. The effect of the remaining amount of the LCs formulations in the stomach on the bioavailability of orally administered PABA was evaluated. The skin permeation and concentration of PABA were also investigated using *in vitro* permeation experiment. As a result, the bioavailability of PABA was significantly improved by administration of PABA-LC formulations compared with that of PABA solution alone, although the remaining effect in the stomach was greatly influenced by the type of LC-forming lipids. The *in vitro* skin permeation study showed that the PABA concentration in skin when applied from the dermis side was higher than when applied from the epidermis side. These findings suggested that oral administration advantageously supports skin drug delivering, and oral LC formulations could be a promising dosage form in cosmeceutical, dietary and clinical fields.

Next, the usefulness of topical LC formulations with skin permeation enhancing ability was investigated. A rather new LC forming lipid, C_{17}-monoglycerol ester (MGE) was evaluated and compared with glycerol monoolate (GMO), which is considered as the gold standard for forming LC formulations. I initially prepared LC formulations containing drugs with different physicochemical properties (tranexamic acid (TXA), 4-methoxy-salicylic acid (4-MS), catechin (CC) and calcein (Cal), and confirmed LC phase structures in the prepared formulations by a polarizing light microscope and a small-angle X-ray scattering (SAXS). Physicochemical properties of these formulations were also performed using a viscometer and a zetasizer. The release rate of the drugs from LC formulations was determined using a

dialysis membrane method. The skin penetration-enhancing ability of LC formulations was also investigated by *in vitro* skin permeation study. The obtained results showed that both MGE and GMO LC forming lipids exhibited the same behavior in terms of their birefringence indices, LC phase structures, particle sizes and zeta potentials. Both the LC formulations consisted of MGE and GMO were managed to improve the skin permeation for various physicochemical properties of drugs. However, MGE formulations showed lower viscosity, faster drug release rate and better skin penetration-enhancing ability than GMO formulations, which strongly suggesting that the low viscosity of LC forming lipid of MGE might influence drug diffusivity and drug permeability through skin. The present MGE-LC formulations can be utilized as a promising new topical formulation for therapeutic drugs and cosmetic ingredients.

Finally, I aimed to develop strategies for designing and optimizing LC formulations to overcome the challenges of poor bioavailable drugs after oral administration and transdermal application by evaluating the physicochemical characterizations of the designed formulations and their ability for *in vitro* and *in vivo* absorption performance. Very limited studies have investigated on the effect of physicochemical properties of entrapped drugs, percentage of LC forming lipids and phase structure of LC formulations on the drug absorption from these formulations after oral or topical administration. In this study, various oral and topical LC formulations were designed based on the changes of LC forming lipid contents in the formulations entrapped with different physicochemical properties of drugs. The obtained results showed that the drug absorption after oral and topical administration of LC formulations were dramatically affected by the percentage of LC forming lipid and physicochemical properties of drugs. An understanding of the effect of such factors could enable us to prepare LC formulations with improved oral absorption and skin permeation of drugs.

General introduction

Liquid crystal (LC) forming lipids represent an important class of biocompatible amphiphiles and their application extends to several fields, such as cosmeceutical, dietary and pharmaceutical technologies. During the last few decades, increasing attention has been paid to the LC formulations including cubosomes and hexosomes because of their remarkable structural complexity and usefulness in diverse application and the LC phases formed by LC forming lipids have been applied to accommodate biologically active molecules such as vitamins, enzymes and other proteins. This ability opens new possibilities for pharmaceutical applications. The advantages of LC formulations as a drug delivery system are their high biocompatibility and self-assembly ability of their structures. This study mainly focuses to overcome the challenges of poorly bioavailable drugs through oral administration and transdermal application using a chemical approach representing by LC formulations. This study is divided in three chapters as follows: the **first chapter** was aimed to develop oral formulations for delivering the drug to skin tissue with a high bioavailability using four different types of LC forming lipid (glyceryl monooleate (GMO), phytantriol (PHT), C_{17}-monoglycerol ester (MGE) and C_{22}-erythritol ester (ERT)) containing a mal-absorptive model compound, *p*-amino benzoic acid (PABA), which is an active element in cosmeceuticals, dietary supplements and skin disorder medicines. The bioavailability and skin concentration of PABA were investigated after oral administration in rats. The **second chapter** of this study was aimed to develop topical LC formulations with skin-permeation enhancing ability. Two different types of LC forming lipids were used: GMO and MGE. GMO is one of the most widely studied LC forming lipids used in the formation of various LC drug formulations; whereas, no studies have utilized the skin-permeation enhancing ability of MGE as a chemical enhancing approach. Both the MGE- and GMO-LC formulations managed to improve the skin-permeation of various drugs with a range of physicochemical properties. However, MGE formulations showed lower viscosity, faster drug release rate and better skin-penetration enhancing ability than GMO formulations, strongly suggesting that the low viscosity of MGE-LC-forming lipids might influence drug diffusivity and permeability through the skin. The present MGE-LC formulation might be

utilized as a promising new topical formulation for therapeutic drugs and cosmetic ingredients. The **third chapter** of this study was aimed to develop strategies for designing and optimizing oral and topical LC formulations by evaluating the effect of several factors such as physicochemical properties of the entrapped drugs and concentration of LC-forming lipids and LC phase structure on the performance of these formulations. Results showed that the concentration of LC-forming lipid and the physicochemical properties of entrapped drugs are key issues for good performance of the LC formulations in various pharmaceutical applications. Understanding the effect of these factors on the LC formulation performance could enable researchers to develop LC formulation approaches that intended to improve the oral absorption and skin-permeation of drugs.

Chapter 1

Usefulness of liquid crystal-oral formulations to enhance the bioavailability and skin tissue delivering of *p*-amino benzoic acid as a model compound

1.1. Introduction

Skin is utilized as an application site for many topical and transdermal drug delivery systems. A variety of topical drug formulations and transdermal drug delivery systems have been developed to treat local indications and systemic diseases. However, topical formulations are not always suitable for treating broad areas of skin, especially in the case of UV protection agents, dietary and cosmetic skin supplements and several skin disorder medicines. Topical application for a broad area skin is often associated with certain drawbacks such as staining of clothes, sweating, pigmentation and skin irritation. Moreover, only a limited number of drugs are amenable to administration by topical application and it is not a practical route to cover large areas of skin on a daily basis [1, 2]. These limitations are associated with a number of drugs not only as medicines for skin disorders but also in dietary and cosmetic skin supplements.

In the present study, I aimed to improve the oral bioavailability and skin tissue delivering of *p*-amino benzoic acid (PABA) as a model compound with a formulation approach by utilizing liquid crystals (LC). LCs are semisolids made of lipids with crystalline structures combining the properties of both crystal and liquid states. Molecules in crystal are highly ordered, while those in liquid are free to diffuse in a random way. Thus, molecules in LC phases diffuse like the molecules in liquid but contain some degree of order [3-6]. A generally used term is the mesophase for LC, indicating such a unique structure is between those of true liquid and solid crystals [7]. In general, LCs can be classified into two categories, *i.e.,* thermotropic and lyotropic. Thermotropic LCs are formed by a change in temperature, whereas lyotropic phases are obtained when mixed with some solvent. Lyotropic LCs usually consist of amphiphilic substances like surfactants and solvents. Amphiphilic substances become micelle at a low concentration, having cluster of molecules with their polar groups oriented in the water. This is a liquid isotropic phase, where isotropic means identical

properties of the structure in all directions. More ordered structures such as hexagonal, lamellar and cubic phases are formed at higher concentrations. These structures are formed, due to insufficient water to fill up spaces between the spherical or elongated micelles [8, 9]. Depending on the solvent concentration and the polarity of solvated mesogen, these systems can undergo phase transitions and structure modifications. Thus, their consistencies and rheological properties can be systematically changed as required [7, 10]. Lyotropic LCs formed with aqueous surfactants can absorb water from the environment, inducing spontaneous phase-transition and forming lamellar phase ($L\alpha$), cubic phase (V_2) and hexagonal phase (H_2) [11, 12]. Among them, cubic phase and hexagonal phase have received much attention due to their highly ordered internal structures, and can be used as a slow release matrix for active pharmaceutical ingredients with various molecular sizes and polarities [13, 14]. Cubic and hexagonal LCs are often spontaneously formed by addition of certain amphiphilic lipids in an aqueous environment [15]. When these LCs are dispersed into nanoparticles by addition of excess water with stabilizers such as Pluronic copolymers and Myrj series [16], they form stable colloidal dispersions which are termed cubosomes and hexosomes, respectively [17-20].

PABA also known as vitamin Bx was selected as a model compound, which is widely found in foods as a cofactor of the vitamin B complex [21]. PABA is often used as an ingredient in sunscreen owing to its high absorbance in the UVB region, and it is protective against skin cancers. Protection against UV and free radical damage is related to the ability of PABA to scavenge reactive oxygen species [22]. It is also available as a health supplement (vitamin B_{10}) because of its antioxidant activity [23]. The potassium salt of PABA is used as a prescription drug in the USA for the treatment of skin disorders such as scleroderma, dermatomyositis and Peyronie's disease [24-26]. Based on these findings, PABA is considered as an active element in cosmeceuticals, dietary supplements and skin disorder medicines. However, PABA suffers from a narrow absorption window in the gastrointestinal (GI) tract [27].

During the last few decades, increasing attention has been paid to LC formulations including cubosomes and hexosomes because of their remarkable structural complexity and

usefulness in diverse applications [28], but very few studies demonstrated their use *in vivo* or particularly for the investigation of their application to oral drug delivery and skin tissue delivering. The first chapter was undertaken with the intention of enhancing the oral delivery and skin tissue delivering of PABA using LC formulations and evaluating LCs as a drug delivery system. Oral LC formulations containing PABA were prepared using the following LC forming lipids: glyceryl monooleate (GMO), phytantriol (PHT), C_{17}-monoglycerol ester (MGE) and C_{22}-erythritol ester (ERT) (Fig. 1-1).

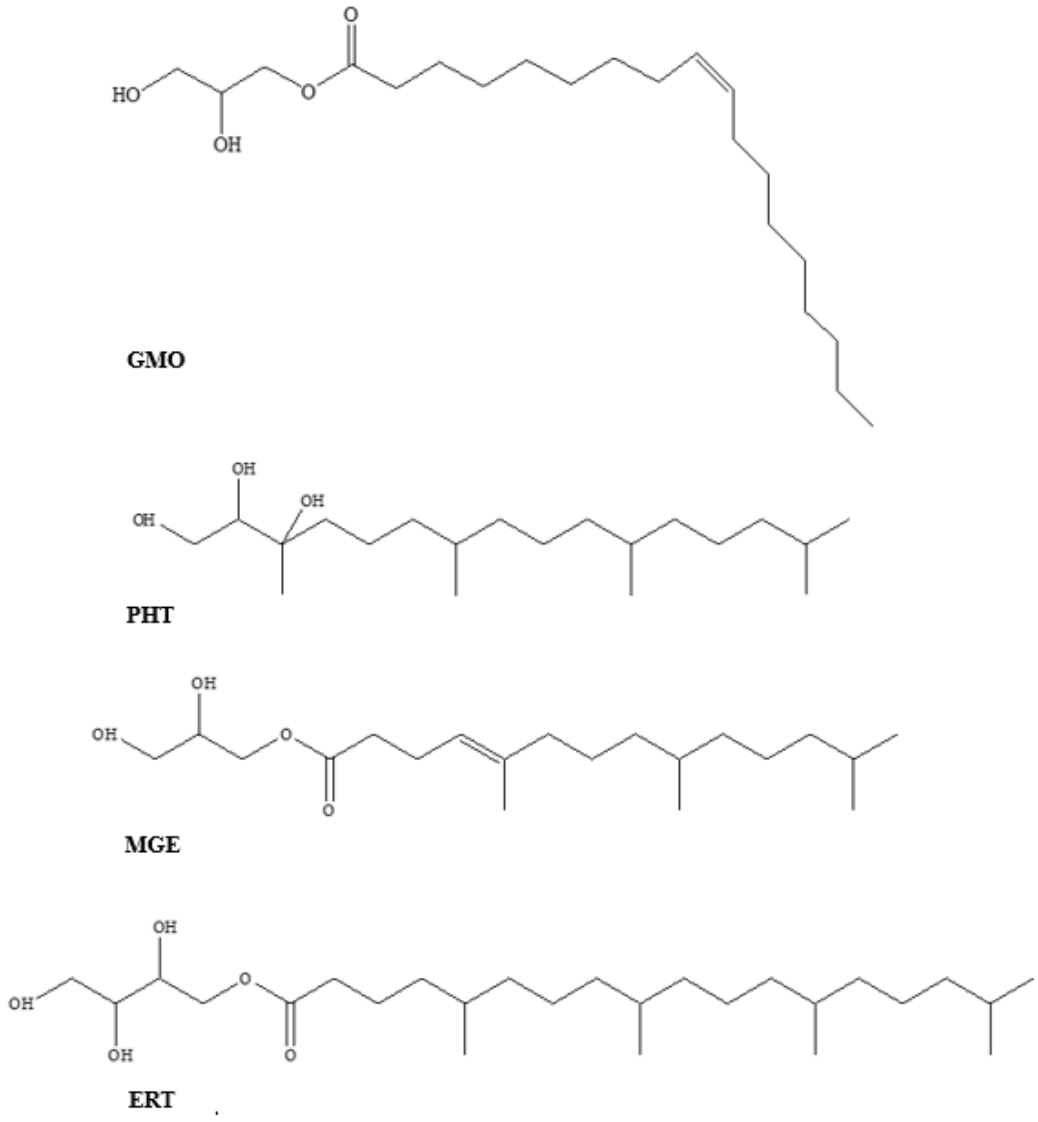

Fig. 1-1. Chemical structures of glyceryl monooleate (GMO), phytantriol (PHT), C_{17}-monoglycerol ester (MGE) and C_{22}-erythritol ester (ERT).

The confirmation of LC phase structures in the presence of PABA was determined by small-angle X-ray scattering (SAXS). The physicochemical measurements of these formulations were performed using a viscometer and a Zetasizer. The *in vitro* release of PABA from LC formulations was determined using a dialysis release method. PABA solution or its dispersed LC formulations were administrated to rats, and the bioavailability, stomach remaining contents and skin concentration of PABA were determined. Furthermore, the skin permeation and concentration were investigated using *in vitro* skin permeation studies.

1.2. Materials and methods

1.2.1. Materials

PABA was purchased from Kanto Chemical Co., Inc. (Tokyo, Japan). GMO with a normal purity of > 97% and MGE with a normal purity of > 99.56% were purchased from Farnex Co., Inc. (Yokohama, Japan). PHT with a normal purity of > 95% and ERT with a normal purity of > 97% were purchased from Tokyo Chemical Industry Co., Ltd. (Tokyo, Japan). A surfactant, Pluronic® F127, was purchased from Sigma-Aldrich (St. Louis, MO, USA). Other reagents and solvents were of special grade or HPLC grade and used without further purification.

1.2.2. Preparation of PABA-LC formulations

Table 1-1 shows the composition of dispersed PABA-LC formulations prepared in this study. These formulations were designed based on a 1:1 ratio of the active ingredient (PABA) solution and LC forming lipids. The mixture was dispersed using an ultrasonic homogenizer (USP-50; Shimadzu Corp., Kyoto, Japan) in a pulsing mode (5-s pulse interrupted by 1-s pauses) for 15 min. GMO was melted at 50°C before use, but ERT was hard to melt even at 100°C. Other LC forming lipids were dispersed with PABA solution without preheating. The dispersion for PABA-GMO, -PHT and -MGE formulations produced uniform opaque creamy mixtures. These formulations were able to be orally administered to rats via an oral zonde needle, although a non-uniform mixture with gel-like

highly viscous aggregates was observed in case of the PABA-ERT formulation. No further work was carried out using PABA-ERT formulation owing to high melting point of ERT.

Table 1-1 Composition of dispersed PABA-LC formulations

Ingredients (%)	PABA-GMO 20 mM	PABA-PHT 20 mM	PABA-MGE 20 mM	PABA-ERT 20 mM
GMO	30	---	---	---
PHT	---	30	---	---
MGE	---	---	30	---
ERT	---	---	---	30
PABA solution	30	30	30	30
Purified water containing 5% Pluronic® F127	40	40	40	40
Total %	100	100	100	100

1.2.3. SAXS measurement

SAXS measurement of dispersed PABA-GMO, -PHT and -MGE formulations was performed using a Nano-Viewer (Rigaku, Tokyo, Japan) with a Pilatus 100K/RL 2D detector. The X-ray source was Cu Kα radiation with a wavelength of 1.54 Å and operating at 45 kV and 110 mA. The sample-to-detector distance was set at 375 mm. Each sample was placed into a vacuum-resistant glass capillary cell and exposed at 25°C for 10 min (Fig. 1-2). The obtained SAXS pattern was plotted against the scattering vector length, $q = (4\pi/\lambda)\sin(\theta/2)$, where θ is scattering angle. The lattice parameter (a) was obtained from the gradient of the plot of q as a function of $\sqrt{h^2+k^2+l^2}$ using the following equation: $q = (2\pi/a)\sqrt{h^2+k^2+l^2}$, where h, k, and l are the Miller indices. The scattering intensity was normalized by decayed direct beam intensity.

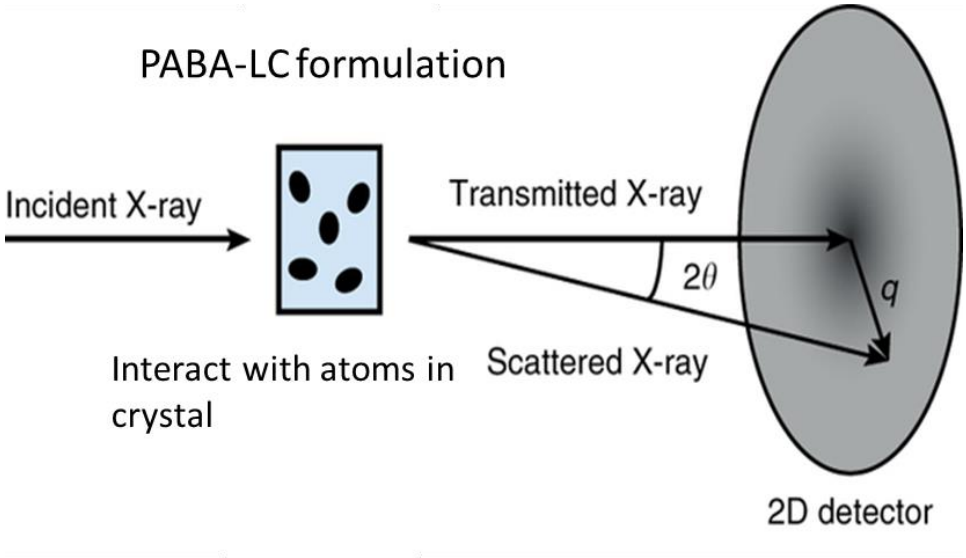

Fig. 1-2. An illustration explains the principle of SAXS.

1.2.4. Measurement of particle size and viscosity

The particle size of LC formulations with or without PABA was measured using a dynamic light scattering Nano-ZS ZEN3600 Zetasizer (Malvern Instruments Ltd., Worcestershire, UK) at 25°C and 37°C. Samples were diluted 10000-fold in water and shaken using a vortex mixer prior to measurement. In addition, the viscosity of LC forming lipids and PABA-LC formulations was measured at 25°C and 37°C using a viscometer (Toki Sangyo Co., Ltd., Tokyo, Japan) that allowed a sensitive determination of viscosity within a range of 0.3-10000 mPa·s with an accuracy of 1% relative error.

1.2.5. Analytical procedures

The *in vivo* or *in vitro* study sample (50 µL) was mixed with the same volume of acetonitrile (to precipitate plasma proteins) containing methyl paraben (10 µg/mL) as an internal standard and centrifuged (5 min, 4°C). The obtained supernatant (20 µL) was injected into an HPLC system. The HPLC system (Shimadzu, Kyoto, Japan) consisted of a system controller (CBM-20A), pump (LC-20AD), auto-sampler (SIL-20AC), column oven (CTO-20A), a UV detector (SPD-M20A), and analysis software (LC Solution). The column was an Inertsil® ODS-3 (5 µm, 4.6 × 250 mm) (Nihon Waters K.K.; Tokyo, Japan), which was maintained at 40°C. The mobile phase was acetonitrile : 0.1% phosphoric acid = 8 : 52 (0-4 min), 35 : 65 (4-14 min) and 8 : 92 (14-20 min). The flow rate was adjusted to 1.0 mL/min. PABA was detected at UV 280 nm. In the case of skin samples, the skin piece (0.1 g) was minced with scissors and homogenized (5 min, 4°C) with water (0.9 mL) using a homogenizer (Polytron PT-MR 3000; Kinematica Inc., Littau, Switzerland). The homogenate was mixed with acetonitrile : water = 1:1 (0.5 mL) and agitated for 15 min. After centrifugation (5 min, 4°C), the supernatant (50 µL) was mixed with the same volume of acetonitrile containing methyl paraben (10 µg/mL) and centrifuged again (5 min, 4°C). The obtained supernatant (20 µL) was injected into an HPLC system, and the measurement was obtained with the same conditions as mentioned above.

1.2.6. *In vitro* dialysis release study

The *in vitro* release study was performed using dialysis bags (Eidia Co., Ltd., Tokyo, Japan). Prior to use, the dialysis bags were soaked in distilled water for 1 h. Phosphate-buffered saline (PBS) as a solvent with physiological pH (7.4) or 0.1 M HCl to simulate gastric conditions (300 mL each) was used as a receiver medium and continuously stirred at 300 rpm in a beaker and warmed in a water bath at 37°C. A dialysis bag was then loaded with 1.0 mL of 20 mM PABA or PABA-LC formulation and placed in the beaker. An aliquot (0.5 mL) was withdrawn from the receiver beaker and the same volume of pH 7.4 PBS or 0.1 M HCl was added to the beaker to keep the volume constant. The concentration of released PABA was then determined using an HPLC in conditions as explained in Section 1.2.5. The

cumulative % PABA release was plotted against the square root of time (Higuchi model) [29].

1.2.7. Animals

Male Wistar rats (200-250 g) were purchased from Sankyo Labo Service Co., Inc. (Hamamatsu, Japan). Male hairless rats were purchased either from Life Science Research Center, Josai University (Sakado, Saitama, Japan) or Ishikawa Experiment Animal Laboratories (Fukaya, Saitama, Japan). Animals were housed in temperature-controlled rooms (25 ± 2°C) with a 12 h light-dark cycle (7:00-19:00 h). The rats were allowed free access to food (Oriental Yeast Co., Tokyo, Japan) and tap water. The animal care protocol was approved by the Animal Care and Use Committee of Josai University (Sakado, Saitama, Japan).

1.2.8. Bioavailability and skin samples excising

Intravenous (*i.v.*) and per oral (*p.o.*) administrations were performed in Wistar rats under anesthesia by intraperitoneal (*i.p.*) injection of three types of anesthesia (medetomidine, 0.375 mg/kg; butorphanol, 2.5 mg/kg; and midazolam, 2 mg/kg) to determine the bioavailability of PABA. In case of *i.v.*, PABA dissolved in physiological saline (PABA solution) was injected (10 μmol/kg) into the tail vein. Blood samples (0.2 mL) were collected from the jugular vein at predetermined intervals up to 3 h, and the same volume of saline was injected via the tail vein to prevent severe changes the in volume of distribution. For *p.o* administration, PABA solution or its dispersed LC-formulation (20 μmol/kg) was administered to rats, and blood (0.2 mL) was sampled from the jugular vein at intervals up to 8 h and the same volume of saline was injected via tail vein. Blood samples placed into heparinized tubes were immediately separated by centrifugation to obtain plasma (5 min, 4°C). Skin samples were taken from the abdomen area at 0.5 or 3 h after *p.o.* administration. Plasma and skin samples were stored at -30°C until analysis.

1.2.9. Determination of PABA concentration remaining in the stomach

Rats were sacrificed at 3 and 8 h after *p.o.* administration of PABA solution or its dispersed LC formulation, and the stomach was removed and the internal lining was scraped with a scalpel blade to collect the stomach contents. The contents were mixed with acetonitrile : ethanol = 2:1 to dissolve the lipid phase and agitated for 15 min. The supernatant (50 µL) after centrifugation (5 min, 4°C) was mixed with the same volume of acetonitrile containing methyl paraben (10 µg/mL) and centrifuged (15,000 rpm, 5 min, 4°C) [28]. The obtained supernatant was diluted 100-fold and injected (20 µL) into an HPLC system. The measurement was obtained as described in Section 1.2.5.

1.2.10. *In vitro* skin permeation study

Full-thickness hairless rat skin was excised from the abdomen under anesthesia by *i.p.* injection of three types of anesthesia (medetomidine, 0.375 mg/kg; butorphanol, 2.5 mg/kg; and midazolam, 2 mg/kg). The excess fat was trimmed off and the skin samples were set in vertical-type diffusion cells (effective diffusion area: 1.77 cm^2) with the epidermis side facing the donor compartment (epidermis to dermis) or facing the receiver compartment (dermis to epidermis). Skin permeation experiments were conducted after hydration for 60 min with PBS pH 7.4 at 32°C. PABA solution (20 mM, 1.0 mL) and PBS (6.0 mL) were added to the donor and receiver compartments, respectively, in all permeation experiments. The receiver solution was agitated using a stirrer bar and a magnetic stirrer throughout the experiments. An aliquot (0.5 mL) was withdrawn from the receiver chamber and the same volume of PBS was added to keep the volume constant. PABA concentration in the receiver was determined using an HPLC as described in Section 1.2.5. The donor solution was removed and the skin sample was washed with PBS after the permeation experiment. The permeation area of the skin (1.77 cm^2) was then cut and stored at -15°C until analysis. The skin concentration was measured as described in Section 1.2.5.

1.2.11. Determination of *AUC*

The area under the plasma concentration-time curve (*AUC*) was calculated using the linear trapezoidal rule. The absolute bioavailability was determined as AUC_{po}/AUC_{iv}, using the mean *AUC* values for *p.o*. and *i.v.* doses. Statistical analysis was performed using unpaired Student's *t*-test (ANOVA), and *P* values less than 0.05 were considered to be significant.

1.3. Results

1.3.1. SAXS evaluation of LC formulations

The phase behavior of dispersed PABA-LC (PABA-GMO, -PHT and -MGE) formulations was evaluated by SAXS. Figure 1-3 shows the X-ray diffraction profiles and the lattice parameter (*a*) of the three PABA-LC formulations. Table 1-2 summarizes the peak position (*q*) and intensity of these formulations. These typical reflection patterns; for dispersed PABA-GMO formulation at nearly √2, √3, √4, √6, √8, √9 (a), PABA-PHT formulation at nearly √2, √3, √4, √6, √8, √9 (b) and PABA-MGE formulation at nearly √2, √3, √4, √6, √8, √9 (c), revealed the presence of inverse bicontinuous cubic (V_2) *Pn3m* phase for the three formulations [30, 31].

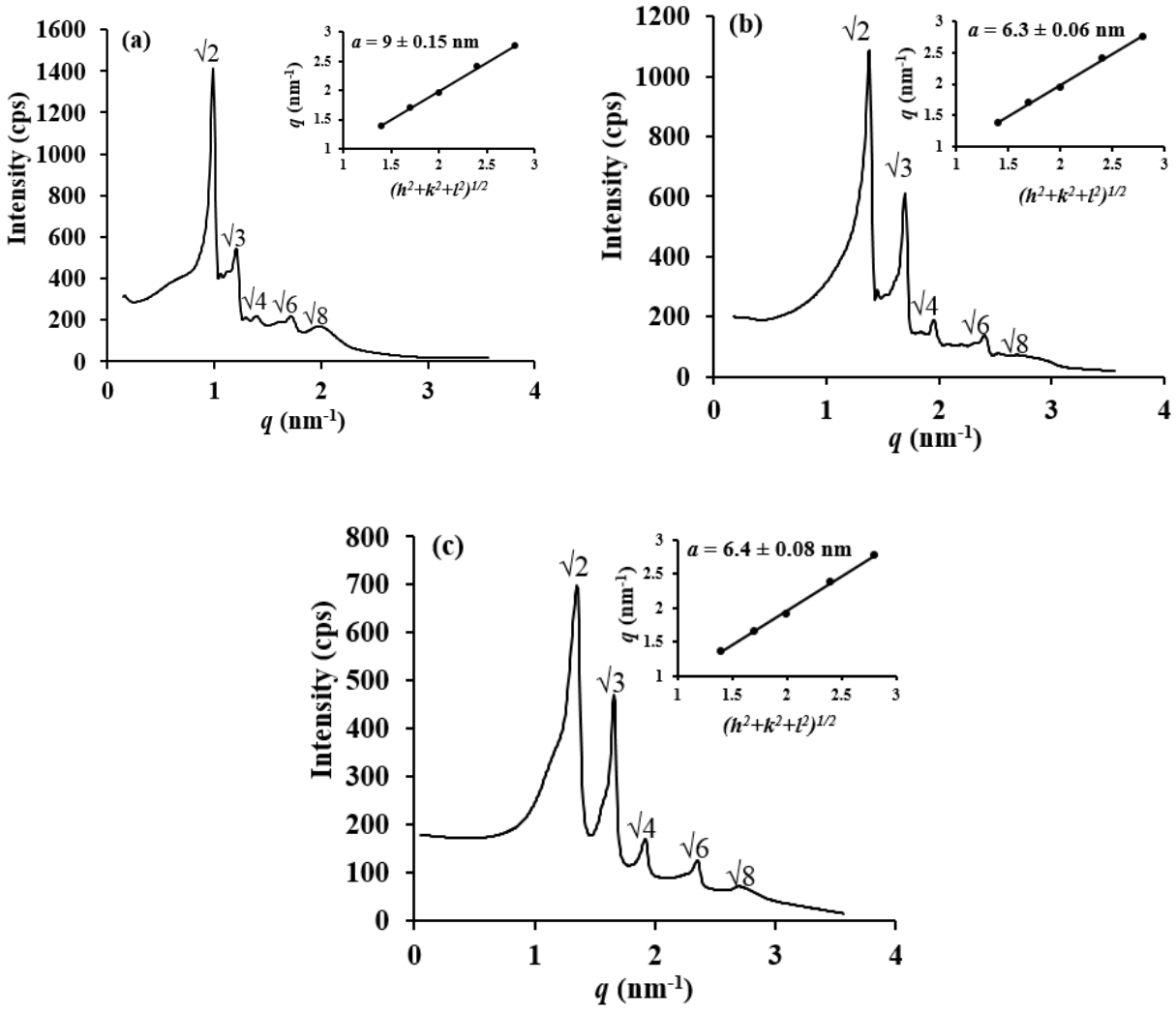

Fig. 1-3. SAXS profiles and lattice parameter (*a*) of PABA-GMO formulation (a), PABA-PHT formulation (b) and PABA-C_{17}-MGE formulation (c).

Table 1-2 Peak position (q) and intensity observed in Bragg reflection of PABA-LC formulations

Formulation	Peak position (q) (nm^{-1})	Intensity (cps)
PABA-GMO	0.982	1412
	1.203	545.8
	1.388	219.8
	1.623	192
	1.979	169
PABA-PHT	1.352	698
	1.659	470
	1.915	169
	2.376	126
	2.772	64
PABA-MGE	1.381	1088
	1.694	609
	1.95	189
	2.406	136
	2.755	69

1.3.2. Particle size and viscosity of LC formulations

The particle sizes of LC formulations with or without PABA in Pluronic® F127 solution were measured by a dynamic light scattering at 25°C and 37°C. Table 1-3 lists the obtained particle sizes. The particle size was nearly 200-400 nm for all formulations, suggesting that the presence of PABA and temperature changes did not affect the particle size of LC formulations.

Table 1-3 Particle size (nm) of LCs

	Dispersed with PABA at 25°C	Dispersed with PABA at 37°C	Without PABA at 25°C	Without PABA at 37°C
GMO	212 ± 15	254 ± 12	244 ± 21	239 ± 23
PHT	332 ± 31	361 ± 34	319 ± 22	352 ± 38
MGE	289 ± 25	320 ± 31	311 ± 27	306 ± 12

Each value represents the mean ± S.E. of 3 experiments.

Moreover, the viscosity of LC forming lipids and their PABA formulations was measured using a viscometer at 25°C and 37°C. Table 1-4 lists the obtained viscosity values. The viscosity grades of LC forming lipids and their PABA formulations were affected dramatically by changes in experimental temperature, except for the MGE-LC forming lipid and its PABA formulation, suggesting that MGE-LC forming lipid is more thermally stable compared with other LC forming lipids.

Table 1-4 Rheological properties of LC forming lipids and LC formulations

	At 25°C	At 37°C
GMO alone*	> 10000	187 ± 23
PHT alone*	8619 ± 34	2019 ± 103
MGE alone*	560 ± 41	175 ± 27
PABA-GMO formulation	6422 ± 133	2193 ± 213
PABA-PHT formulation	7231 ± 183	4331 ± 198
PABA-MGE formulation	1890 ± 201	1101 ± 112

*: LC forming lipid only without water or any additive.

Each viscosity (mPa.s) represents the mean ± S.E. of 3 experiments.

1.3.3. *In vitro* drug release from LC formulations

The *in vitro* release study was performed using dialysis bags. PBS as a solvent with physiological pH (7.4) or 0.1 M HCl for gastric conditions was used as the receiver medium. Figure 1-4 shows PABA release profiles from LC formulations into PBS pH 7.4 (a) and 0.1 M HCl (b). The PABA release profile into 0.1 M HCl was similar to that when PBS was used as the receiver medium, indicating that changes in pH probably did not affect the release rate of PABA from its solution or its LC formulations. The PABA release profile from the LC formulations was a relatively slow and gradual till 60 min compared with that from PABA solution. The release profiles of PABA from its GMO and MGE formulations were similar each other. Higuchi's square-root model analysis showed two phases of PABA release; a fast release phase (5-60 min), followed by a slow release phase (60-240 min) of PABA from the LC-matrix. The correlation coefficients of PABA-LC formulations were calculated in accordance with the release profiles obtained using square root Higuchi model as shown in Table 1-5.

The amount of PABA released from GMO, PHT and MGE were 81 ± 3, 67 ± 2 and 90 ± 4%, respectively, against the initial dosing. These results showed that the release profile of PABA from the PHT formulation was slower than that from other PABA-LC formulations and could be related to its high viscosity at 37°C, which could lead to reduced mobility of PABA in this formulation compared with other PABA-LC formulations.

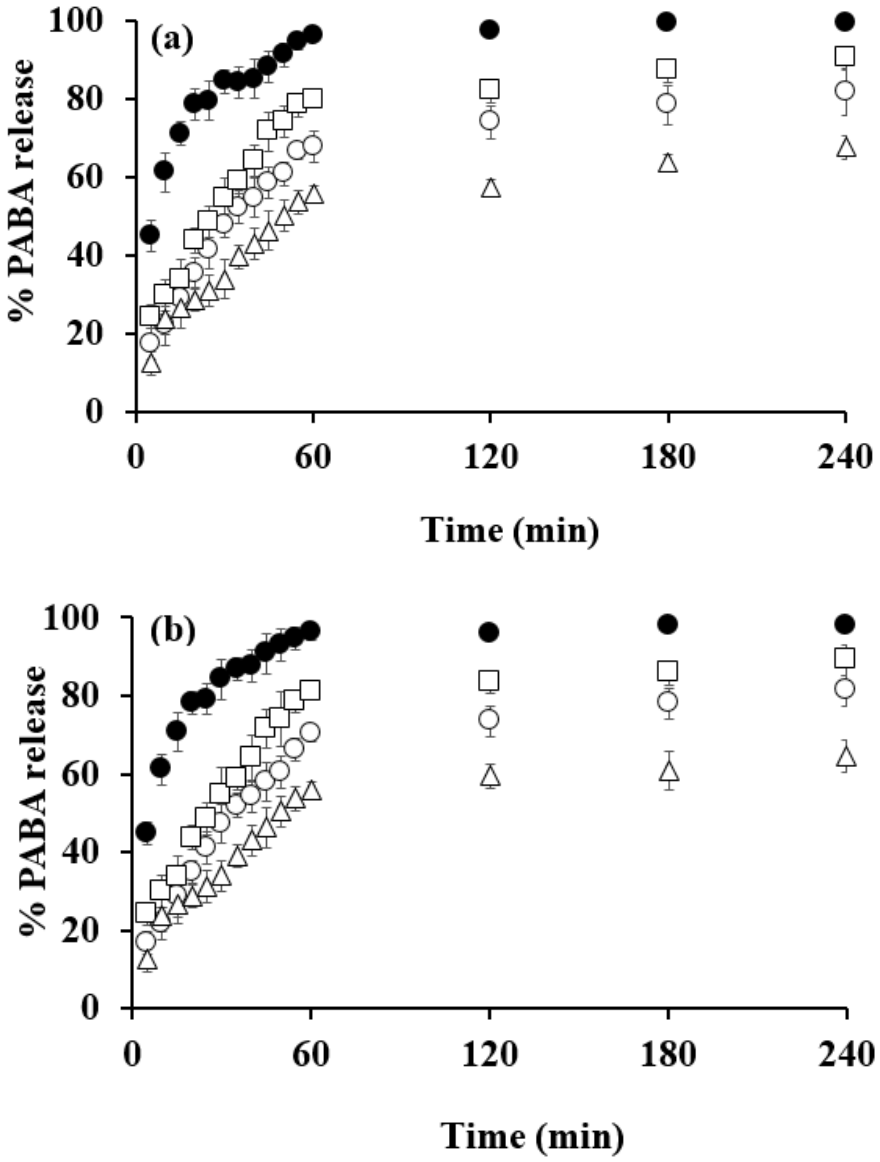

Fig. 1-4. Percentage of *p*-amino benzoic acid (PABA) release profiles into phosphate-buffered saline (PBS) pH 7.4 (a) and 0.1 M HCl (b). Symbols: (●), PABA solution; (○), PABA-glyceryl monooleate (GMO) formulation; (△), PABA-phytantriol (PHT) formulation; and (□) PABA-C_{17}-monoglycerol ester (MGE) formulation. Each point represents the mean ± S.E. of three experiments.

Table 1-5 Correlation coefficients* of PABA-LC formulations

	Fast release phase (pH 7.4)	Slow release phase (pH 7.4)	Fast release phase (0.1 M HCl)	Slow release phase (0.1 M HCl)
PABA-GMO	0.9965	0.9993	0.9965	0.9992
PABA-PHT	0.9902	0.9974	0.9937	0.9904
PABA-MGE	0.9936	0.9973	0.9881	0.9791

*: The correlation coefficients were obtained by data from 5-60 and 60-240 min as a represent to the fast release phase and the slow release phase, respectively.

1.3.4. Bioavailability of PABA after oral administration of LC formulations

Figures 1-5 and 1-6 show the time course of the plasma concentration of PABA after *i.v.* and *p.o.* administration of its solution or LC formulations in male Wistar rats, respectively. Table 1-6 summarizes the calculated $AUC_{0\text{-}6\ h}$, T_{max}, C_{max} and bioavailability of PABA after administration of PABA solution or its dispersed LC formulations. The C_{max} after oral administration of dispersed PABA-MGE or -GMO formulations was significantly higher than with PABA solution. The T_{max} for administration of dispersed PABA-MGE formulation was faster compared with PABA solution and other PABA-LC formulations. In addition, the bioavailability of PABA was significantly improved by administration of dispersed PABA-MGE or -GMO formulations compared with PABA solution. Although the PABA-PHT formulation resulted in a significant improvement in bioavailability, a relatively lower C_{max} was obtained compared with the other formulations. No plasma concentration was observed 6 h after administration except for the PHT formulation, for which a very low concentration of PABA (3 ± 1 nmol/mL) was observed at 8 h (not shown in Fig. 1-6).

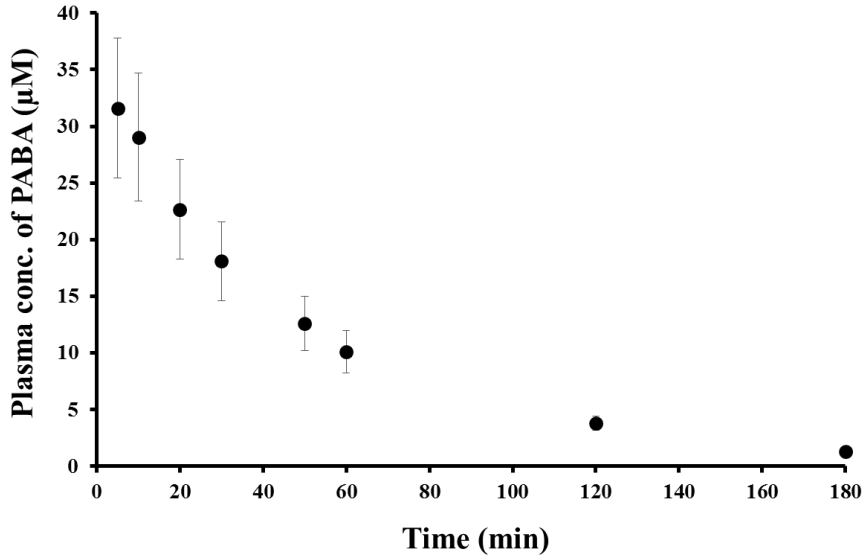

Fig. 1-5. Plasma profile after intravenous injection of PABA.

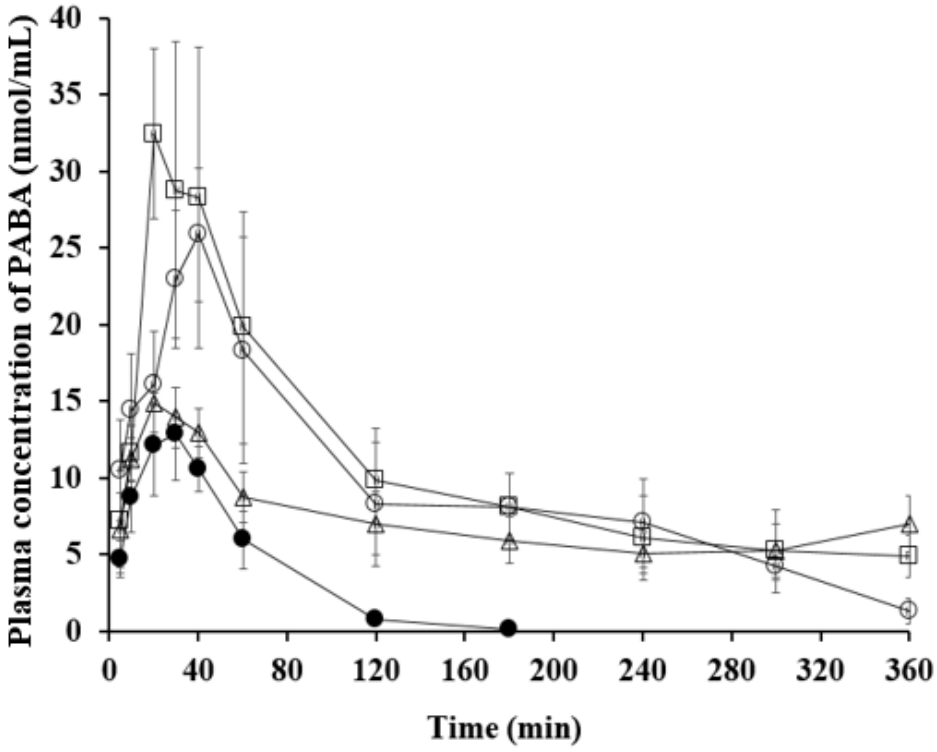

Fig. 1-6. Plasma profiles of PABA after oral administration. Symbols: (●), PABA solution; (○), PABA-GMO formulation; (△), PABA-PHT formulation; and (□) PABA-MGE formulation. Each point represents the mean ± S.E. of three experiments.

Table 1-6. Bioavailability of PABA after oral administration of its solution or its dispersed LC formulation

	$AUC_{0\text{-}6\ h}$	T_{max} (min)	C_{max} (μM)	Bioavailability $_{0\text{-}6\ h}$ (%)
PABA solution	774 ± 77	33 ± 5	13 ± 2.3	19 ± 2
GMO-PABA	3203 ± 107*	38 ± 5	27 ± 2.4*	78 ± 3*
PHT-PABA	1467 ± 98*	30 ± 8	15 ± 0.89	62± 10*
MGE-PABA	3887 ± 539*	26 ± 9	36 ± 3.7*	91 ± 13*

Each value shows the mean ± S.E. of 3 experiments.

*: $P < 0.05$ significantly different from PABA solution (Student's *t*-test).

1.3.5. Skin concentration of PABA

Figure 1-7a and b show the skin concentration of PABA 30 min and 3 h, respectively, after oral administration of PABA solution or its dispersed LC formulation. A significant improvement in the skin concentration at 30 min was observed with the GMO and MGE LC formulations compared with PABA solution, but no improvement was observed using the PHT formulation. No detection of PABA in skin was observed 3 h after application of PABA solution. However, LC formulations sustained a low concentration of PABA in the skin even 3 h after administration. These results suggested that GMO and MGE formulations were more efficient for enhancing the skin concentration of PABA than PABA solution and PHT formulation.

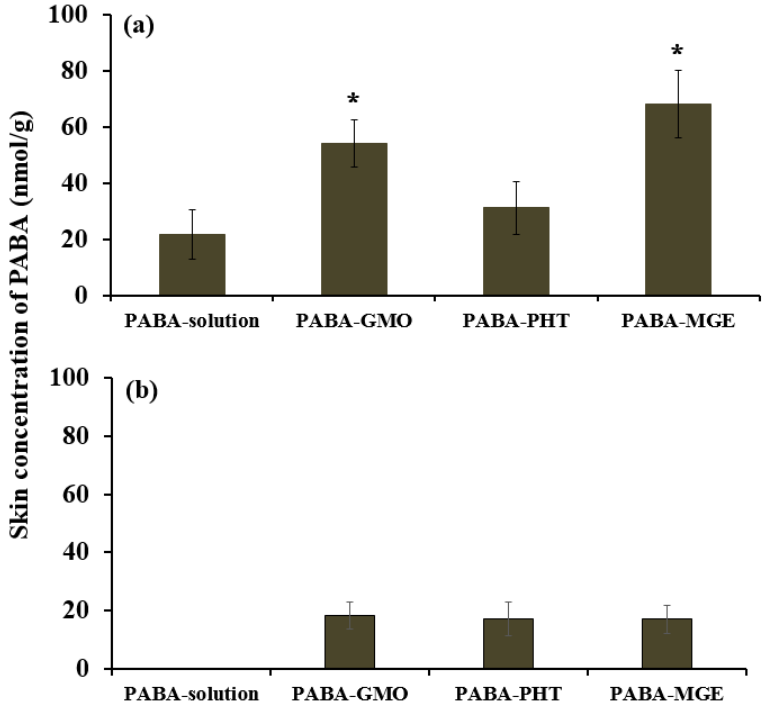

Fig. 1-7. Skin concentration of PABA: (a) 30 min after oral administration of PABA solution or its LC formulation; (b) 3 h after oral administration of PABA solution or its LC formulation. Each column represents the mean ± S.E. of three experiments. *: $P < 0.05$ significantly different from PABA solution (Student's *t*-test).

1.3.6. Concentration of PABA remaining in the stomach

In order to estimate the sustained release of PABA from LC formulations, the PABA concentration remaining in the stomach was determined 2 and 8 h after *p.o.* administration of its solution or LC formulation. LC dispersions were observed to accumulate in the pyloric region of the stomach, as shown in Fig. 1-8. Figure 1-9 shows nearly 40% of the total dose of PABA concentration from the PHT formulation remained in the stomach 2 h after administration, and nearly 20% remained from the GMO and MGE formulations (Fig. 1-9a). No PABA was detected 8 h after administration of PABA solution or GMO and PHT formulations, but nearly 12% of the total dose of PABA in the PHT formulation remained in the stomach 8 h after administration (Fig. 1-9b). The high percentage of PABA remaining in

the stomach for the PHT formulation must be consistent with its high viscosity, leading to a prolonged emulsification effect of the formulation in the stomach.

Fig. 1-8. An illustrative photograph of the remaining dispersed PABA-LC formulation in the stomach of rats after oral administration.

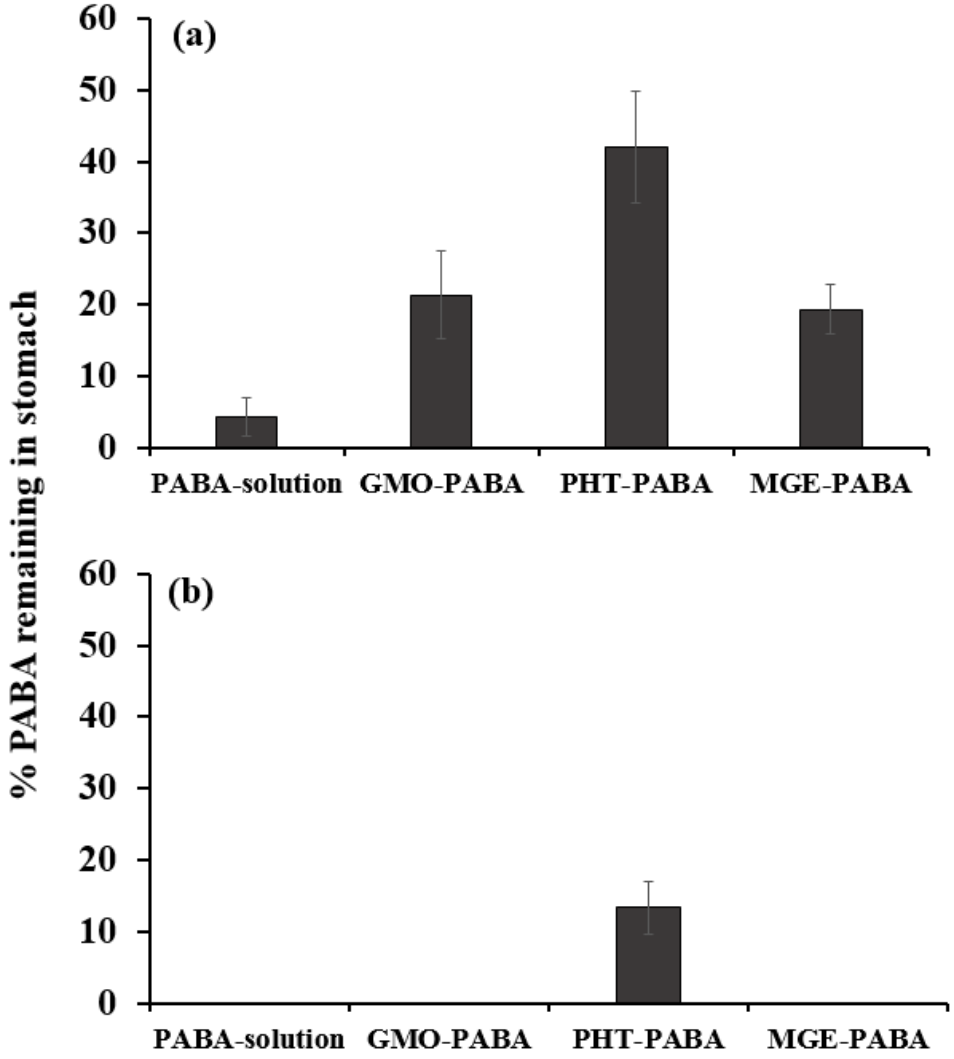

Fig. 1-9. The percentage of PABA remaining in the stomach: (a) 2 h after oral administration of PABA solution or its dispersed LC formulation; (b) 8 h after oral administration of PABA solution or its dispersed LC formulation. Each column represents the mean ± S.E. of three experiments.

1.3.7. *In vitro* skin permeation study

Figure 1-10 shows the time course of cumulative amount of PABA that permeated through the full-thickness skin of hairless rats. Almost no change was observed in the skin permeation profile of PABA after application to the epidermis side or the dermis side. However, PABA skin concentration was significantly higher when applied on the dermis side compared with the epidermis-side application, as shown in Fig. 1-11. This indicated that the partition of PABA to skin tissue from the dermis side was higher than that from the epidermis side; and this supported for usefulness of *p.o.* administration, especially for delivering of PABA to the skin.

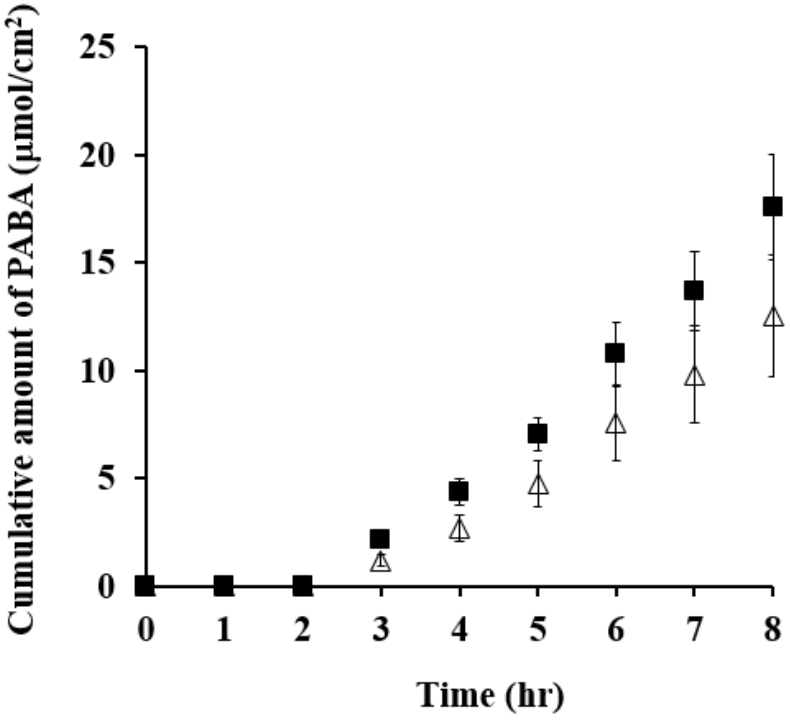

Fig. 1-10. *In vitro* skin permeation study: time course of the cumulative amount of PABA that permeated through full-thickness hairless rat skin. Symbols: (■), from the dermis to epidermis; and (△), from the epidermis to dermis. Each point shows the mean ± S.E. of three experiments.

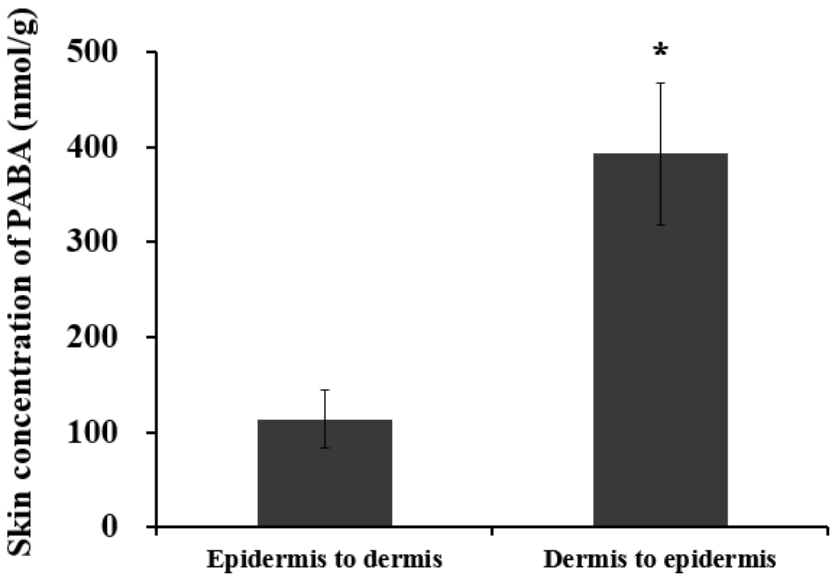

Fig. 1-11. Skin concentration of PABA after an 8 h *in vitro* skin permeation experiment. Each column represents the mean ± S.E. of three experiments. *: $P < 0.05$ significantly different from the epidermis to dermis (Student's *t*-test).

1.4. Discussion

The general concept of delivering the skin tissue is by topical application. Very limited studies have emphasized drug-skin tissue delivering via oral administration. The issue to be addressed in this study is that the skin is the largest organ in our body and it is not always suitable to distribute an active ingredient over the whole area of the skin especially for certain indications. Hence, it is necessary to develop oral-skin tissue delivery systems that can effectively deliver a drug to a wide area of skin. Recent studies have shown successful development of LC formulations that can be applicable for *i.v.* administration [32, 33]. A previous study [32] has demonstrated that PHT dispersions could trigger complement activation, and the process may limit their use for *i.v.* administration as this may initiate infusion-related reactions in sensitive individuals. However, complement activation was significantly milder when PHT was replaced with GMO. These finding should be considered for the safety concerns of such materials. Minimal studies have been undertaken to

investigate potential toxic effects of nanoparticle formulations made from LC forming lipids [34-36]. GMO was reported as a nontoxic, biodegradable and biocompatible material classified as GRAS (generally recognized as safe), and it is included in the FDA *Inactive Ingredients Guide* and in non-parenteral medicines licensed in the UK [37]. Its biodegradability comes from the fact that GMO is subject to lipolysis due to diverse kinds of esterase activity in different tissues [38-40]. In contrast, PHT comprises of a trihydroxy head group and a branched phytanyl tail without the presence of a labile (*e.g.* ester) functionality, which may confer more stable toward enzymatic degradation [41, 42]. A previous study has showed that the *in vitro* toxicity of PHT cubosomes is considerably greater than that of GMO cubosomes. The increased toxicity of PHT appears to result from its greater ability to disrupt the cellular membrane and oxidative stress [42]. No toxicity studies have been reported to investigate the toxic effect of MGE cubosomes. Further efforts are necessary to investigate the potential toxicity of such materials for therapeutic applications.

In the present study, I evaluated LC forming lipids formulations as an orally administered drug delivery system for skin tissue delivering. I initially prepared PABA oral formulations using different types of LC forming lipids. The phase behavior of these formulations was determined by SAXS measurement, based on international tables for crystallography [30, 31] obtained reflection patterns for dispersed PABA-GMO formulation at √2, √3, √4, √6, √8, √9 (Fig. 1-3a), PABA-PHT formulation at √2, √3, √4, √6, √8, √9 (Fig. 1-3b) and PABA-MGE formulation at √2, √3, √4, √6, √8, √9 (Fig. 1-3c), thereby confirming the presence of inverse bicontinuous cubic (V_2) *Pn3m* phase for the prepared formulations (Table 1-2). These results are consistent with previous studies on GMO and PHT [43-45]. In addition, the obtained lattice parameters (*a*) of PABA-GMO formulation (Fig. 1-3a) and PABA-PHT formulation (Fig. 1-3b) are consistent with other studies on GMO and PHT [46, 47]. In case of MGE (Fig. 1-3c), no studies were reported on its formulations phase behavior.

The particle sizes of the LC formulations with or without PABA were measured at 25°C and 37°C. The obtained data showed that the particle size was not affected by changes in temperature or the presence of PABA dispersion (Table 1-3). Although the particle size of

the GMO formulation with or without PABA was smaller compared with other LC formulations, the details were unknown.

The viscosity grade of LC forming lipids and their PABA formulations was dramatically decreased at physiological temperature (37°C) except for MGE and its PABA formulation, which showed almost similar grades at 25°C and 37°C (Table 1-4). The reason why the viscosity grade of GMO at 25°C was expressed as >10,000 mPa.s was due to the viscometer allowing a sensitive determination of viscosity within a range of 0.3-10,000 mPa·s. These results suggested that MGE is more thermally stable than GMO and PHT LC forming lipids.

In vitro dialysis release studies showed that there were no changes in the release profiles of PABA in PBS pH 7.4 (Fig. 1-4a) and in 0.1 M HCl (Fig. 1-4b), suggesting that changes in the physiological GI tract pH do not affect the release behavior of PABA. The amount of PABA released from its GMO and MGE formulations was 81 ± 3 and 90 ± 4%, respectively, against a dose at 240 min. In case of PABA-PHT formulation, PABA release was slower than that from the PABA solution or other PABA-LC formulations and the amount of PABA released was 67 ± 2% at 240 min. These results suggested that the high viscosity of PHT at 37°C could affect the drug mobility in its formulation and its release rate. High correlation coefficients were obtained for each formulation as shown in Table 1-5, which indicated that *in vitro* drug release profiles of PABA cubosomes were fitted well with the square root Higuchi model. The obtained two phases of PABA release suggested a proposed diffusion mechanism that PABA tends to be adsorbed at the surface of LC during the fast release phase (5-60 min), followed by a slow release phase (60-240 min) of PABA from the LC-matrix. In-depth investigations, the short time taken to achieve more than 50% release of PABA from its LC formulations justifies that these systems are a burst release delivery system where drug is released by diffusion from the cubic phase matrix. Other studies also showed that cubosomes should be classified as a burst release delivery system [8, 48].

In vivo studies have shown that the bioavailability of PABA was significantly improved by administration of PABA-LC formulations compared with PABA solution alone (Fig. 1-6 and Table 1-6). The C_{max} after oral administration of dispersed PABA-MGE (36 ± 3.7 nmol/mL) or -GMO (27 ± 2.4 nmol/mL) formulation was significantly higher than PABA solution (13 ± 2.3 nmol/mL). The T_{max} after administration of dispersed PABA-MGE (26 ± 9 min) formulation was relatively faster compared with PABA solution (33 ± 5 min) and the PABA-GMO (38 ± 5 min) and -PHT (30 ± 8 min) formulations. In addition, the bioavailability of PABA was significantly improved by administration of dispersed PABA-MGE (91 ± 13%) or -GMO (78 ± 3%) formulations compared with PABA solution (19 ± 2%). Although the PABA-PHT formulation exhibited significantly improved bioavailability (62 ± 10%), no significant improvement in C_{max} was obtained compared with those for PABA solution and the other formulations. No plasma concentration was observed 6 h after administration except for the PHT formulation, in which a very low concentration of PABA (3 ± 1 nmol/mL) was observed at 8 h (not showed in Fig. 1-6). These results suggested that the PABA-MGE formulation was the most efficient formulation for enhancing C_{max} and the bioavailability of PABA. Although the PABA-PHT formulation managed to sustain PABA concentration even at 6 h after administration, the C_{max} was not improved compared with the PABA solution only. In addition, the obtained results suggested that changes in the bioavailability can be observed dependent on the individual LC forming lipid used in the formulation (Fig. 1-6). Further investigations was done to examine the effect of the physiological temperature, viscosity and the emulsifying effect of the stomach on the bioavailability of PABA. The PABA-PHT formulation showed the highest viscosity at 37°C compared with the other formulations, which was consistent with the high percentage of PABA remaining in the stomach with this formulation compared with the other PABA-LC formulations (Fig. 1-9). Because the emulsifying ability of the stomach is well known [45], the obtained results suggested that the high viscosity of PHT could delay the emulsifying rate of the PABA formulation in the stomach and consequently could prolong the absorption rate and stomach emptying rate of the dispersed drug. This could be a reason why it managed to

sustain the release of PABA for longer hours but with relatively low bioavailability and C_{max} compared with the other formulations.

The other LC forming lipids used in this study was GMO, which is one of the most widely studied LC forming lipids [49]. The present findings showed that the physical state of GMO can be easily affected with the changes in temperature and the viscosity of this LC forming lipid and its PABA formulation was dramatically decreased at 37°C. In addition, the amount of PABA remaining in the stomach using GMO was low compared with the PABA-PHT formulation. These results suggested that this formulation can be emulsified by the stomach at a faster rate compared with PABA-PHT, and this might offer better drug mobility and influence the movement and absorption of the drug in the intestine. Therefore, it significantly improved bioavailability and C_{max} compared with PABA solution. At the same time, the high viscosity of this LC forming lipid at 25°C makes it not easy to handle, not practical for drug loading and need to melt at 50°C before its use.

In the case of MGE, no studies have utilized this for oral drug delivery. The present finding showed that MGE was more thermally stable compared with other LC forming lipids. The PABA-MGE formulation showed the highest bioavailability and C_{max} and relatively short T_{max} compared with PABA solution and other LC formulations. The low viscosity of MGE at 37°C might offer more drug mobility and drug absorption from the intestine, and this was consistent with the low amount of PABA remaining in the stomach compared with PABA-PHT the formulation (Fig. 1-9), at the same time its low viscosity at 25°C makes it easy to handle and more practical for drug loading.

In consequence, a non-uniform mixture with gel-like high viscosity aggregates was observed in the preparation of the PABA-ERT formulation, which was related to the high melting point of ERT, making it impractical for designing an oral formulation; therefore, no further work was carried out using this lipid.

Although a significant improvement in skin concentration was observed with the administration of dispersed PABA-GMO or -MGE LC formulations compared with PABA solution at 30 min, no significant enhancement in the skin concentration of PABA was

observed using PABA-PHT formulation compared with PABA solution (Fig. 1-7a). No detection of PABA in the skin was observed 3 h after PABA solution administration. However, dispersed PABA-LC formulations maintained a low concentration of PABA in the skin even after 3 h (Fig. 1-7b). As a consequence, as shown in Fig. 1-6 and Table 1-6, the C_{max} of PABA after *p.o.* administration of its solution or LC formulations was obtained within 40 min after administration, then the concentration profiles of PABA decreased after 40 min. In addition, the skin concentrations at 30 min were higher than those at 3 h after administration. These results suggested that the skin concentrations of PABA were closely related to its plasma level.

Moreover, *in vitro* skin permeation results showed no changes in the skin permeation profiles of PABA after application of its solution on the epidermis side or on the dermis side (Fig. 1-10). However, skin concentration of PABA was significantly higher after its application on the dermis side compared with its application on the epidermis side (Fig. 1-11), indicating that the affinity of PABA for accumulation in the skin via systemic direction is higher than its delivery via the topical direction; and this could be due to the high barrier function of the stratum corneum. The results obtained in this study advantageously support the concept of delivering PABA to skin.

1.5. Chapter conclusion

The present data showed that LC formulations are a promising approach to improve the oral absorption and skin tissue delivering of PABA. The PABA-MGE formulation was the most efficient formulation for enhancing C_{max}, bioavailability and skin tissue delivering of PABA compared with other formulations. The plasma concentration profiles can be modified based on the type of LC forming lipid used in the formulation design. Despite the changes in the plasma concentration profiles that the observed using different LC forming lipids, my main intention was to enhance the oral absorption and skin tissue delivering of PABA and to evaluate LC formulations for oral drug delivery. Further studies need to be conducted to investigate the mechanism of enhancing GI tract-drug absorption using LC formulations. Delivering the drug to skin by orally dispersed PABA-LC formulations could be a promising achievement in cosmeceutical, dietary and clinical fields.

Chapter 2

A novel chemical enhancer approach for transdermal delivery with C_{17}-monoglycerol ester liquid crystal forming lipid

2.1. Introduction

Transdermal administration of drugs represents an excellent alternative to conventional pharmaceutical dosage forms. Transdermal delivery provides convenient and pain-free self-administration for patients. It eliminates frequent dosing administration and peaks and troughs in plasma level associated with oral dosing and injections to maintain a constant drug concentration, so that drugs with a short half-life can be delivered effectively by transdermal administration. However, transdermal drug delivery often faces the problem of no or insufficient penetration of the active pharmaceutical substances through the skin. The outermost layer of skin, the stratum corneum, has a role as the primary barrier against water evaporation from the body and drug entry through skin into the body. Thus, overcoming the stratum corneum barrier is important to develop transdermal drug delivery systems. Chemical approaches, such as penetration enhancers [50] and physical approaches, such as iontophoresis [51], phonophoresis [52] and electroporation [53, 54], have been evaluated to increase the skin permeation of several drugs. Physical approaches are often associated with several disadvantages, such as their requirement for special application apparatus and their cost. Therefore, in the present study I aimed to evaluate the chemical or formulation approach with skin permeation-enhancing ability using LC formulation. LCs are semisolids made of lipids with crystalline structures combining the properties of both crystal and liquid states. GMO (Fig. 1-1) is one of the most widely studied LC-forming lipids used for topical application, and it is considered the gold standard for developing LC formulations [55, 56]. In the present study, I investigated the skin penetration enhancing effect of a novel LC-forming lipid, MGE (Fig. 1-1), and the results obtained were compared with those with GMO. Although previous studies have provided information on LC formulations for

transdermal drug delivery [4, 57], very few studies have focused on the skin penetration-enhancing ability of LC-forming lipids with different physicochemical properties of drugs.

GMO is a very well-known self-assembling amphiphilic molecules that form a variety of crystalline structures with useful mechanical properties of special interest in drug delivery. In the presence of a small amount of water, GMO forms reversed micelles characterized by an oily texture [58]. As more water is added, a mucous-like system is formed that corresponds to the lamellar phase. GMO forms cubic or hexagonal phases when more water is added (20-40%) over a wide temperature range. These phases are highly viscous, in the presence of high amounts of water in temperatures ranging from 20-70 °C, the cubic and hexagonal phases might exist in a stable condition [59, 37]. Previous research has demonstrated that the LC phases of GMO such as the cubic and hexagonal phases, increased transdermal drug delivery. As a transdermal absorption enhancer, GMO probably acts by causing a temporary and reversible disruption of the lamellar structure of the lipid bilayer in the stratum corneum and, in this way, increasing intercellular lipid fluidity [60, 61].

In the present study, I initially prepared LC formulations containing drugs with different physicochemical properties (tranexamic acid [TXA], 4-methoxy-salicylic acid [4-MS], catechin [CC], and calcein [Cal]) (Table 2-1). These formulations were prepared using two different types of LC-forming lipids: MGE and GMO. The chemical structures of MGE and GMO are showed in Fig. 1-1. As mentioned above, GMO is the most widely studied LC-forming lipid, but no previous studies have utilized the skin permeation enhancing ability of MGE.

Table 2-1 Physicochemical properties of the compounds used in the present study.

	Abbreviation	M.W.	log $K_{o/w}$*
Tranexamic acid	TXA	157.21	-0.3
4-Methoxy-salicylic acid	4-MS	152.14	0.5
Catechin	CC	290.26	0.8
Calcein	Cal	622.55	-2.02

* Octanol/water partition coefficient of compounds at pH 7.4

The confirmation of LC phase structures in the prepared formulations was determined using a polarizing light microscope and SAXS. The physicochemical measurements of these formulations were performed using a viscometer and a Zetasizer. The release of drugs from LC formulations was determined using a dialysis release method. The skin penetration-enhancing ability of LC formulations was also investigated by *in vitro* skin permeation studies.

2.2. Materials and methods

2.2.1. Materials

MGE with a normal purity of > 99.56% and GMO with a normal purity of > 97% were obtained from Farnex Co., Inc. (Yokohama, Japan). TXA was purchased from Sigma Aldrich (St. Louis, MO, USA). 4-MS, CC, and Cal were purchased from Tokyo Chemical Industry Co., Ltd. (Tokyo, Japan). Other reagents and solvents were of special grade or HPLC grade and used without further purification.

2.2.2. Preparation of LC formulation

Table 2-2 shows the composition of LC formulations prepared in this study (for chapter 2). These formulations were designed based on a 1:1 ratio of the active ingredient in distilled water (drug solution) and LC-forming lipids. GMO was melted at 70°C before use, but MGE was dispersed with drugs solution without preheating. The mixture was dispersed

using a microsyringe dispenser (250 µL-syringe) (Ito Corporation, Shizuka, Japan).

Table 2-2 Composition of dispersed TXA-, 4-MS-, CC-, and Cal-LC formulations.

Formulation	Drug concentration	% Drug solution	% MGE	% GMO
TXA-MGE	19 mM	50	50	---
4-MS-MGE	1 mM	50	50	---
CC-MGE	10 mM	50	50	---
Cal-MGE	3 mM	50	50	---
TXA-GMO	19 mM	50	---	50
4-MS-GMO	1 mM	50	---	50
CC-GMO	10 mM	50	---	50
Cal-GMO	3 mM	50	---	50

2.2.3. Polarizing light microscopic examination

The LC samples were observed using a polarizing light microscope (Olympus IX71, Tokyo, Japan). A pin-tip amount of the LC-forming lipid or LC formulation was smeared onto a microscope glass slide using a microsyringe dispenser and then quickly covered with a cover slip. The microsyringe containing LC-forming lipid or LC formulation was slowly pressed over the glass slide to make it as thin as possible. GMO was melted at 70°C before pressing it over the glass slide, but MGE was pressed without preheating. A 40× objective lens and 10× eyepiece lens were used with cross polarizers in the bright field to detect birefringence. Micrographs were taken using the polarizing microscope.

2.2.4. Measurement of particle size and zeta potential

The particle size and zeta potential of LC formulations were determined using a dynamic light scattering Nano-ZS ZEN3600 Zetasizer (Malvern Instruments Ltd., Worcestershire, UK). LC samples were diluted in water and shaken using a vortex mixer prior to measurement. Following the particle size analysis of the LC formulations, the mode

was switched from ‘‘Size’’ to ‘‘Zeta,’’ and the zeta potential of the LC formulations was recorded. Each measurement for the particle size and zeta potential was repeated three times.

2.2.5. Measurement of viscosity

The viscosity of LC-formulations was measured using a viscometer (Toki Sangyo Co., Ltd., Tokyo, Japan) that allowed a sensitive determination of viscosity within a range of 0.3–10,000 mPa·s with an accuracy of 1% relative error.

2.2.6. SAXS measurement

SAXS measurement of LC-formulations was performed using a Nano-Viewer (Rigaku, Tokyo, Japan) with a Pilatus 100K/RL 2D detector. The X-ray source was Cu Kα radiation with a wavelength of 1.54 Å and operating at 45 kV and 110 mA. The sample-to-detector distance was set at 375 mm. Each sample was placed into a vacuum-resistant glass capillary cell and exposed at 25°C for 10 min. The SAXS pattern obtained was plotted against the scattering vector length, $q = (4\pi/\lambda)\sin(\theta/2)$, where θ is the scattering angle.

2.2.7. Release study

A dialysis membrane (molecular weight cut-off; 2,000–14,000 Da) (Sanko Junyaku Co., Tokyo, Japan) was set in a vertical-type diffusion cell (effective diffusion area: 0.95 cm^2) and the receiver chamber was maintained at 32°C. Phosphate-buffered saline (PBS; pH 7.4) was applied to the receiver chamber for TXA, 4-MS, and CC, and PBS containing 1.0 mM EDTA·2Na was used for Cal. Drug solution (1.0 mL) or its LC formulation (300 mg) was applied to the donor cell to start the release experiment. An aliquot (500 µL) was withdrawn from the receiver chamber, and the same volume of PBS or 1.0 mM EDTA·2Na was added to the chamber to keep the volume constant. The amount of TXA, 4-MS and CC released was determined using an HPLC (Shimadzu Ltd., Kyoto, Japan). In case of Cal, the amount released was determined using a fluorescence spectrophotometer (Shimadzu Ltd., Japan). The cumulative % drug release was plotted against the square root of time (Higuchi’s law) [29].

2.2.8. Animals

Male hairless rats (8 weeks old) were purchased either from Life Science Research Center, Josai University (Sakado, Saitama, Japan) or Ishikawa Experiment Animal Laboratories (Fukaya, Saitama, Japan). Animals were housed in temperature-controlled rooms (25 ± 2°C) with a 12 h light-dark cycle (07:00–19:00 h). The rats were allowed free access to food (Oriental Yeast Co., Tokyo, Japan) and tap water. The animal experiment protocol was approved by the Animal Care and Use Committee of Josai University (Sakado, Saitama, Japan).

2.2.9. *In vitro* skin permeation study

Full-thickness hairless rat skin was excised from the abdomen under anesthesia by *i.p.* injection of three types of anesthesia (medetomidine, 0.375 mg/kg; butorphanol, 2.5 mg/kg; and midazolam, 2 mg/kg). The excess fat was trimmed off and the skin samples were set in vertical-type diffusion cells (effective diffusion area: 0.95 cm^2) with the epidermis side facing the donor compartment. PBS (pH 7.4) with or without 1.0 mM EDTA·2Na was applied to the receiver chamber as in the release experiment and maintained at 32°C. These skin permeation experiments were conducted after hydration for 60 min with PBS with or without 1.0 mM EDTA·2Na. Drug solution (1.0 mL) or its LC-formulation (300 mg) was applied to the donor cell to start the *in vitro* skin permeation experiment. An aliquot (500 µL) was withdrawn from the receiver chamber, and the same volume of PBS with or without 1.0 mM EDTA·2Na was added to the chamber to keep the volume constant. The skin permeation of TXA, 4-MS and CC permeated through skin was determined by HPLC, and that of Cal was determined using a fluorescence spectrophotometer.

2.2.10. HPLC conditions

The same volume of acetonitrile containing parabens was added to TXA, 4-MS and CC samples. After gentle mixing, the sample was centrifuged for 5 min at 21,500 × g and 4°C to remove proteins and contaminants. The supernatant was injected onto the HPLC. The

HPLC system consisted of a pump (LC-10AD; Shimadzu, Kyoto, Japan), Chromatopac (C-R6A; Shimadzu), UV detector (SPD-6A; Shimadzu), system controller (SCL-6B; Shimadzu), and auto-injector (SIL-7A; Shimadzu). The LiChroCART®250-4 column (KGaA·64271; Merck, Darmstadt, Germany) was maintained at 40°C during the eluting mobile phase, 0.1% phosphoric acid:acetonitrile = 75:25 for TXA, 0.1% phosphoric acid:acetonitrile = 55:45 for 4-MS, and 0.1% phosphoric acid containing 5 mM sodium dodecyl sulfate:acetonitrile = 50:50 for CC. The flow rate was adjusted to 1.0 mL/min. The injection volume was 20 μL, and detection was performed at 220 nm for TXA, 230 nm for 4-MS and 245 nm for CC.

2.3 Results

2.3.1 Polarizing light microscopic examination

Figures 2-1 and 2-2 shows samples observed using a polarizing light microscope. No optical anisotropy was observed in cases of MGE and GMO alone (a, b), because these lipids cannot form crystalize structures without excess amount of water. In case of MGE- and GMO-LC formulations, they showed clear optical anisotropy on the displayed image (c, d, e, f, g, h, i, j). Moreover, these formulations appeared as uniform opaque ointment-like mixtures with no visible signs of aggregates.

In general, if there was any materials with high birefringence, the light output by the top layer, a linear polarizer, may cause optical anisotropy to appear on the displayed image, depending on the orientation of the viewer with respect to the display. These results showed that the present LC formulations were managed successfully to form crystallized formulations because of high birefringence with the polarizing light microscope.

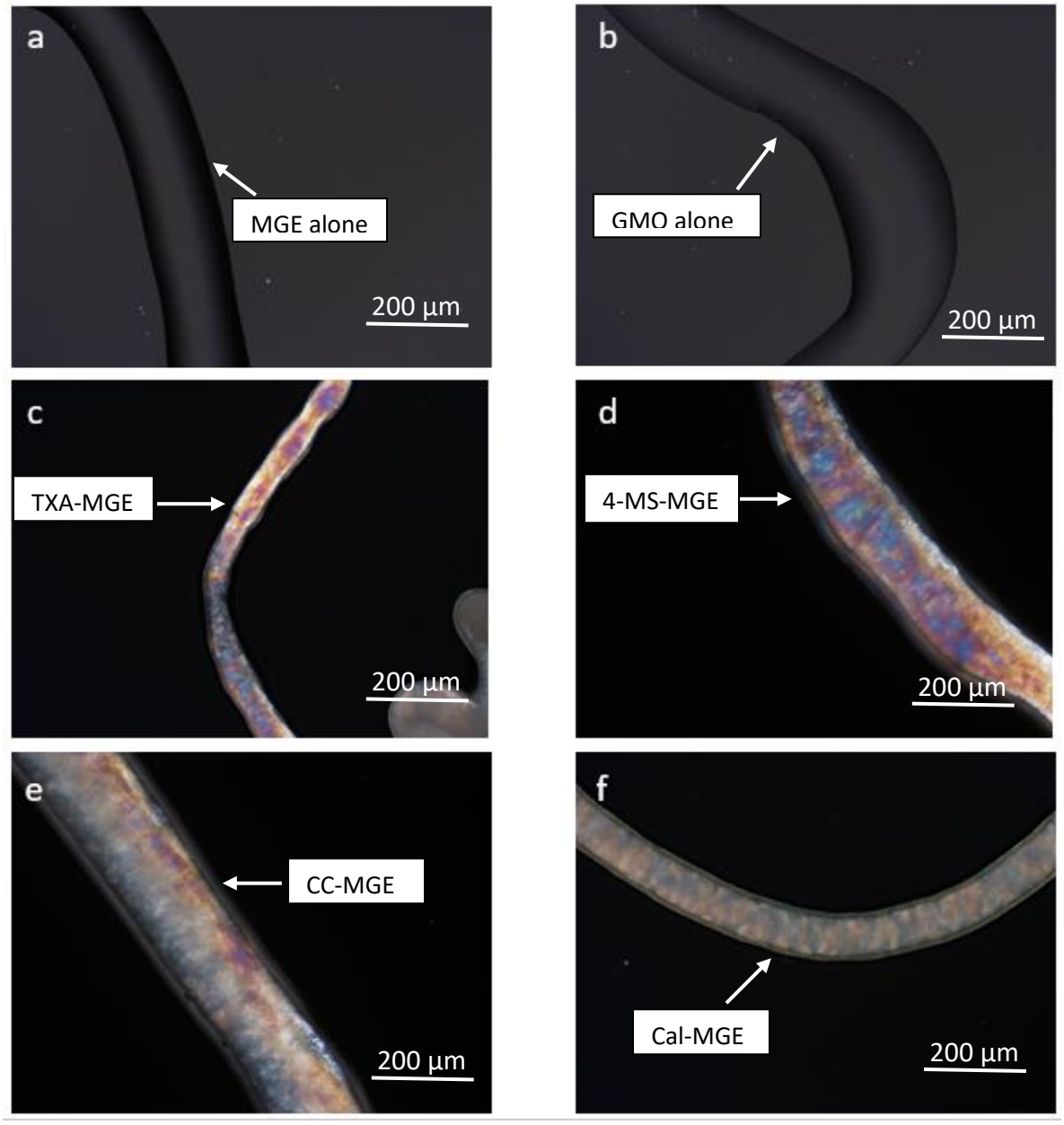

Fig. 2-1. LC-forming lipids or LC formulations upon application under polarized microscope: (a), MGE alone; (b), GMO alone; (c), TXA-MGE formulation; (d), 4-MS-MGE formulation; (e), CC-MGE formulation; (f), Cal-MGE formulation. The optical anisotropy confirming the presence of LC in the prepared formulation.

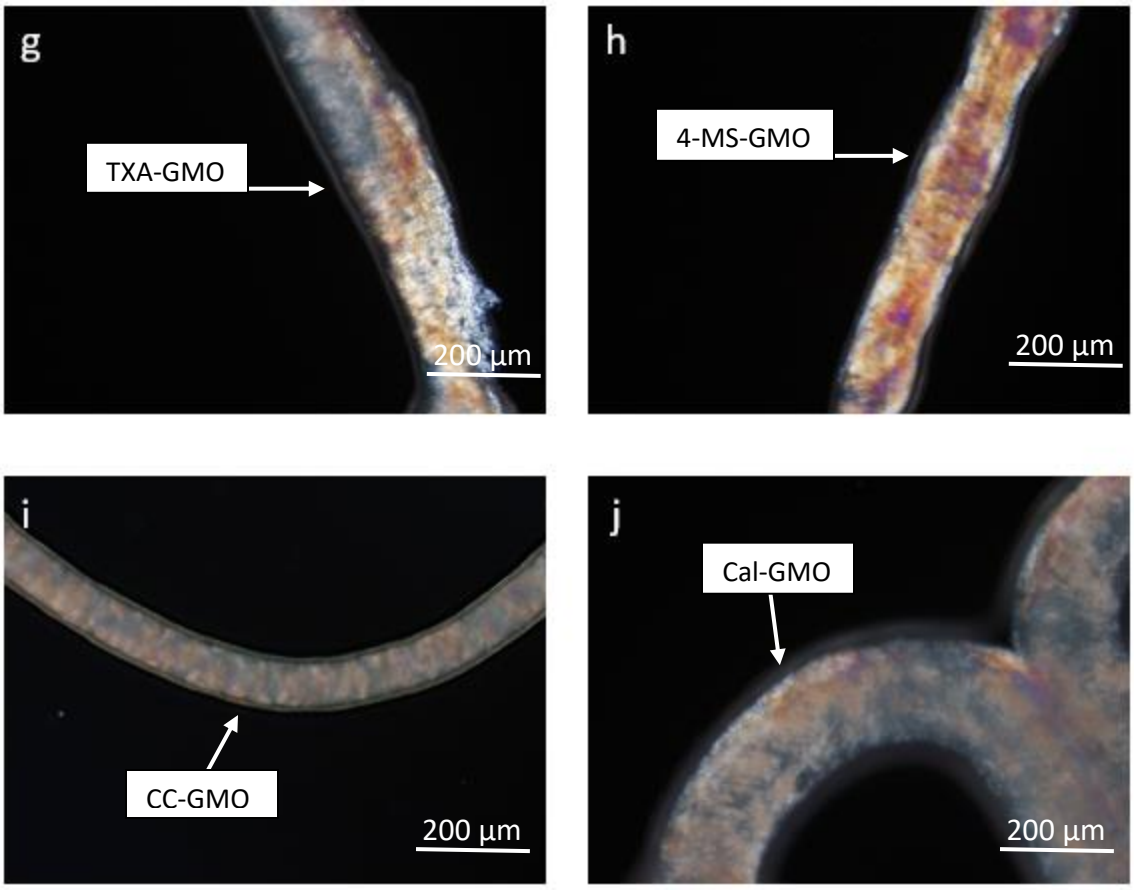

Fig. 2-2. LC-forming lipids or LC formulations upon application under polarized microscope: (g), TXA-GMO formulation; (h), 4-MS-GMO formulation; (i), CC-GMO formulation and (j), Cal-GMO formulation. The optical anisotropy confirming the presence of LC in the prepared formulations.

2.3.2. SAXS chart of LC formulations

The phase structure of TXA-, 4-MS- and CC-MGE and GMO formulations was evaluated by SAXS. Figure 2-3 shows the X-ray diffraction profiles of all the formulations. The typical reflection patterns at nearly 1, √3, and √4 revealed the presence of a hexagonal phase (H_1, H_2) in all prepared formulations (a-d) (e-h in Appendix / Supplementary data) [30, 31]. These results confirmed that both MGE- and GMO-LC formulations managed to form hexosomes successfully.

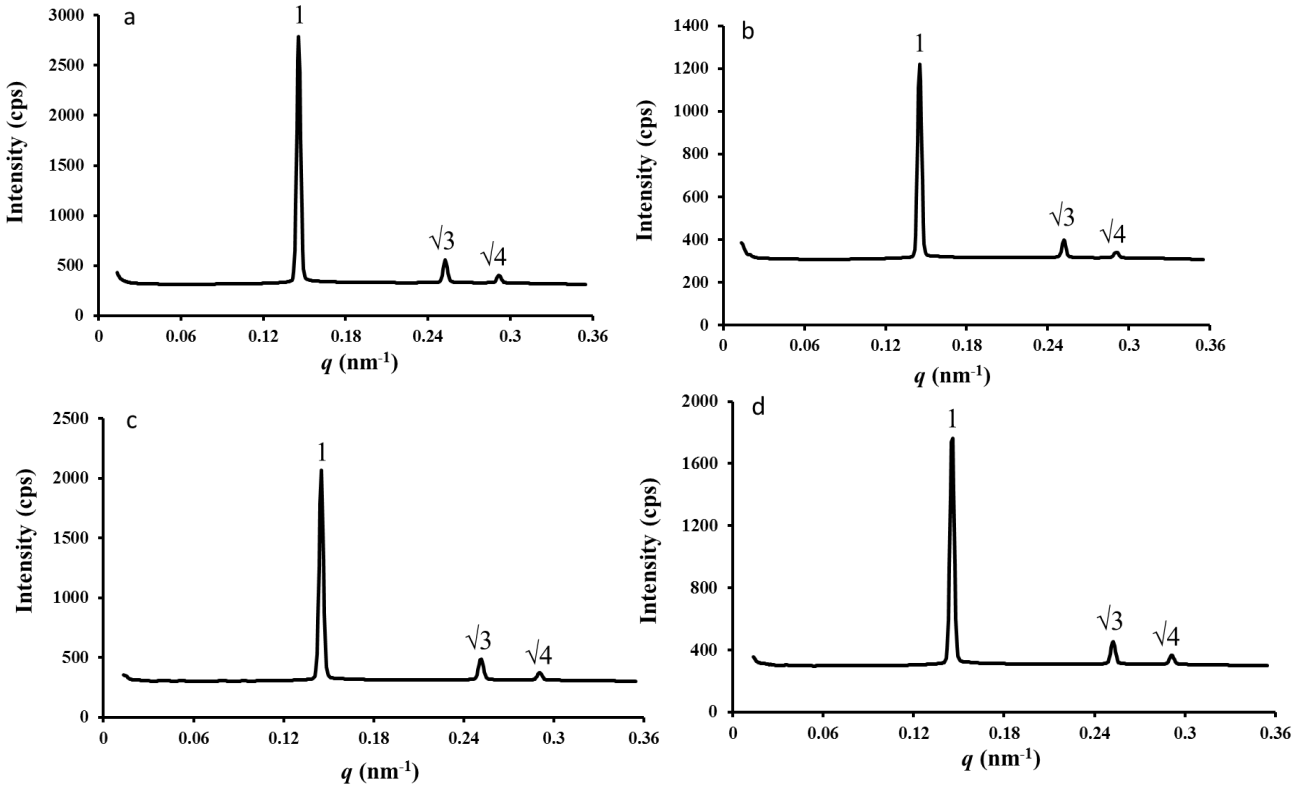

Fig. 2-3. SAXS charts of LC formulations.

(a), TXA-MGE formulation; (b), 4-MS-MGE formulation; (c), CC-MGE formulation; (d), Cal-MGE formulation; (e), TXA-GMO formulation; (f), 4-MS-GMO formulation; (g), CC-GMO formulation and (h), Cal-GMO formulation. The reflection patterns at: 1, √3, √4 confirming the presence of a hexagonal phase (H_1, H_2) for all prepared formulations (a-d) (e-h in Appendix / Supplementary data).

2.3.3. Measurement of particle size and zeta potential

The particle size and zeta potential of LC formulations were determined immediately (Fig. 2-4a, b) and 10 days (Fig. 2-4c, d in Appendix / Supplementary data) after their preparation. The results showed that both MGE- and GMO-LC formulations had small particle sizes ranged between 220 and 280 nm, and the zeta potential of these formulations was ranged between -17 and -30 mV. In addition, no significant changes were observed in particle size or zeta potential at 10 days after their preparation.

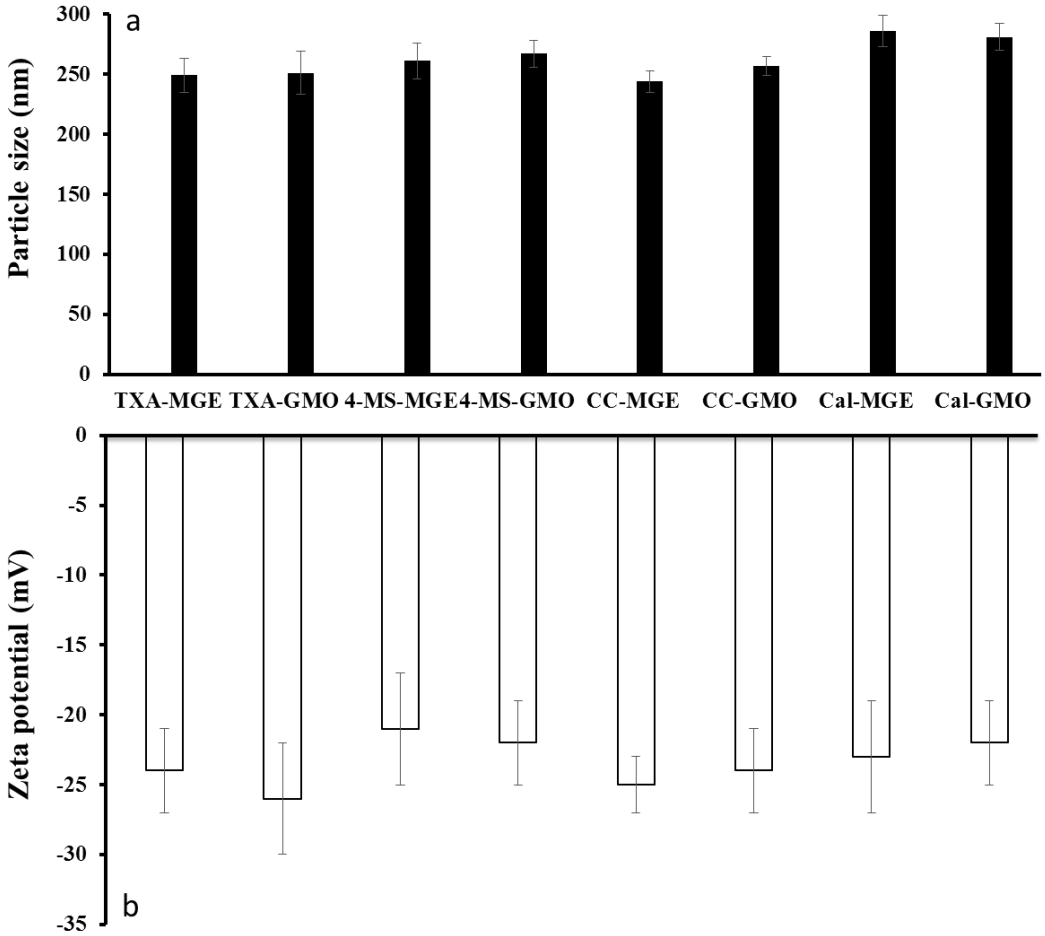

Fig. 2-4. Particle size (a, c) and zeta potential (b, d) of LC formulations immediately (a, b) and 10 days (c, d in Appendix / Supplementary data) after preparation. Each point represents the mean ± S.E. of three experiments.

2.3.4. Measurement of viscosity

The viscosity of LC formulations was measured using a viscometer. Figure 2-5 shows the obtained viscosity values. These values were affected dramatically by the type of LC-forming lipids used in the preparation. The viscosity values of LC formulations with MGE were significantly lower than those with GMO. These results showed that MGE-LC-formulations has lower viscosity than GMO-LC-formulations, and its low viscosity made it easy to handle and more practical for drug loading. GMO requires melting at 70°C before its use for formulation preparation, but MGE was dispersed with drug solution without preheating owing to its low viscosity.

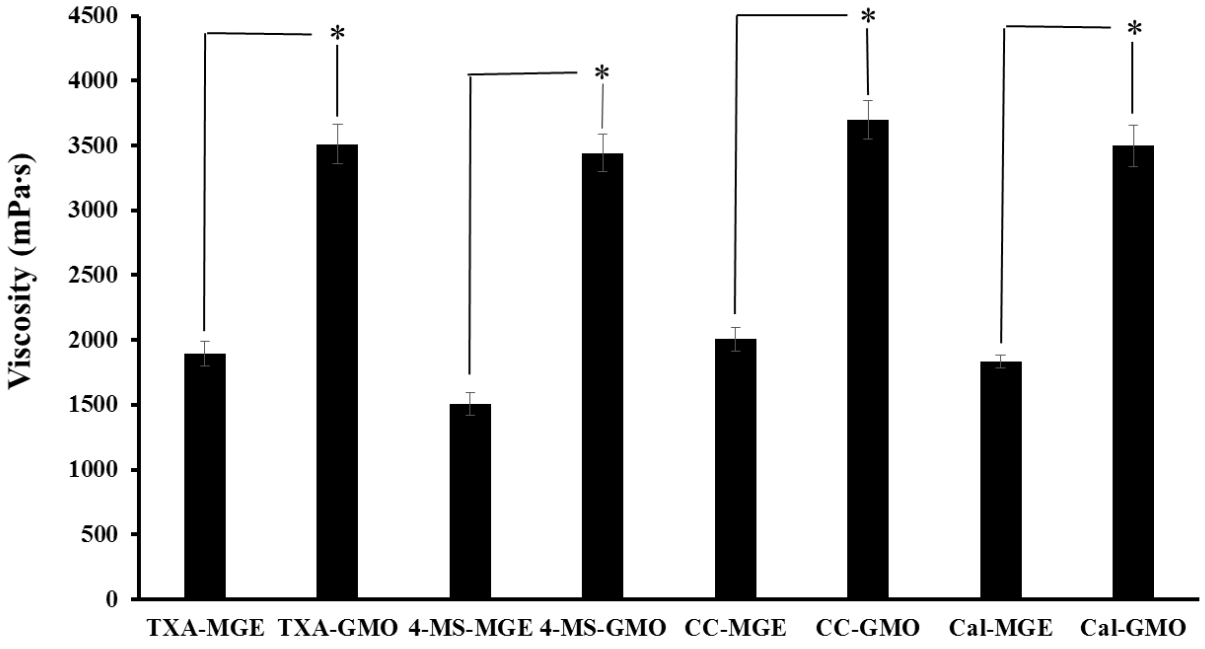

Fig. 2-5. The apparent viscosity of LC formulations.

Each point represents the mean ± S.E. of three experiments.*: $P < 0.05$ significantly different from MGE-LC formulation (Student's *t*-test).

2.3.5. Drug release properties from LC formulations

The release study was performed using a vertical-type diffusion cell. Figure 2-6 shows the release profile of TXA, 4-MS, CC and Cal from their MGE and GMO formulations. All profiles were obeyed to Higuchi's law [29]. The amounts of TXA, 4-MS, CC and Cal released from MGE formulations were 13.9 ± 2.5%, 23.7 ± 3.2%, 16.7 ± 2.8%, and 9.6 ± 0.8%, respectively, against the initial dosing. In the case of GMO formulations, the amounts of TXA, 4-MS, CC and Cal released were 7.3 ± 1.6%, 14.4 ± 2.2%, 10 ± 1.8% and 6.1 ± 0.9%, respectively, against the initial dosing. These results might be related to the high viscosity of GMO-LC formulations and thus could affect the drug diffusivity and the release rate.

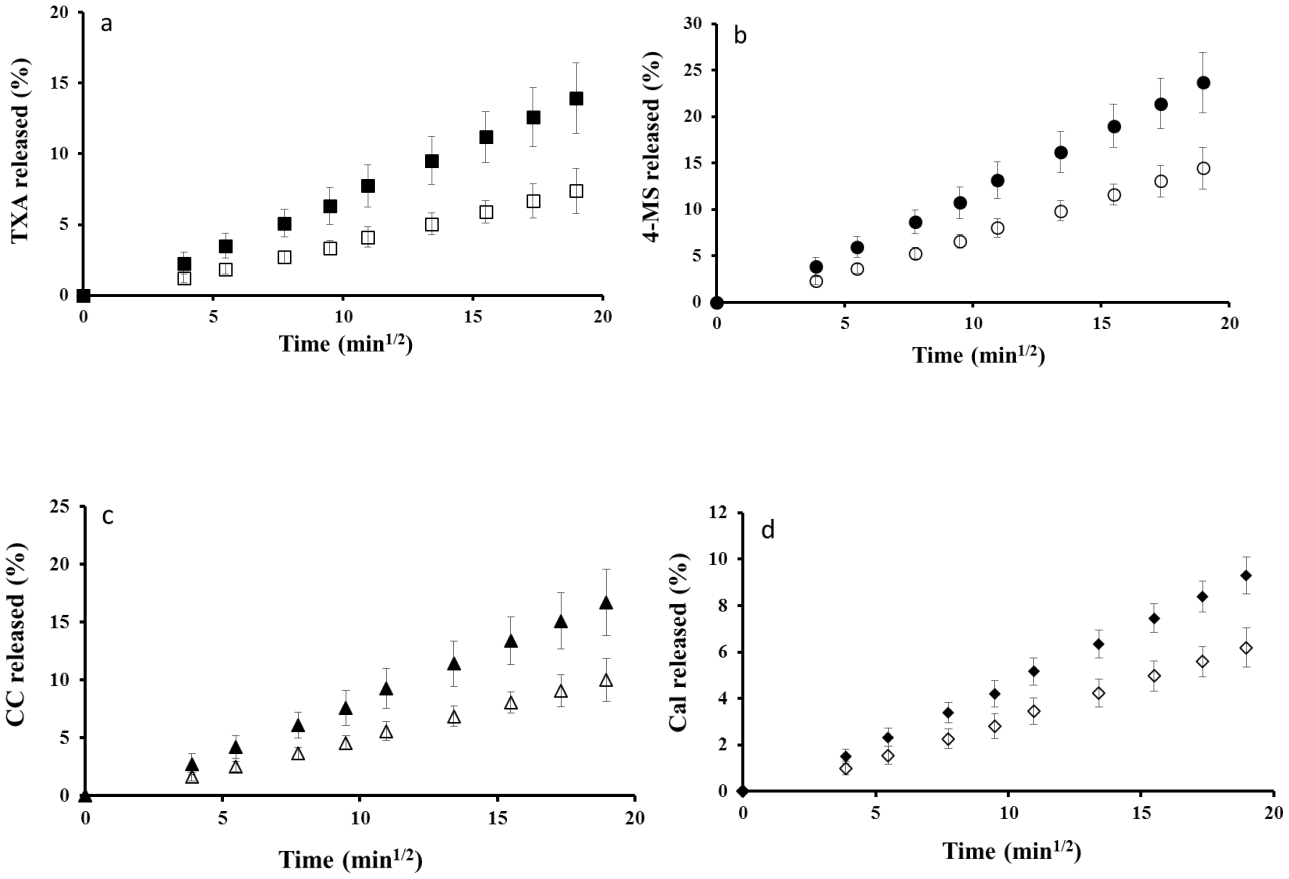

Fig. 2-6. Release profiles of TXA (a), 4-MS (b), CC (c) and Cal (d) from their LC formulations. Symbols: (a): (■), TXA-MGE formulation; (□), TXA-GMO formulation; (b): (●), 4-MS-MGE formulation; (○), 4-MS-GMO formulation; (c): (▲), CC-MGE formulation; (△) CC-GMO formulation; (d): (◆), Cal-MGE formulation; (◇), Cal-GMO formulation. Each point represents the mean ± S.E. of three experiments.

2.3.6. Skin permeation of drugs from LC formulations

Figure 2-7 shows the effect of MGE and GMO formulations on the time course of the cumulative amount of TXA, 4-MS, CC, and Cal that permeated through hairless rat intact skin. Significant improvements in skin permeation of TXA, 4-MS, and CC were observed after application their MGE and GMO formulations compared with that permeated from drug solution (dissolved in water). The enhancement skin permeation ratios for TXA-, 4-MS-, CC-, and Cal-MGE formulations were 4.6, 3.5, 4.2, and 5.5, respectively, and those for TXA-, 4-MS-, CC-, and Cal-GMO formulations was 2.5, 2.6, 3.1, and 3, respectively. These results clearly showed that MGE formulations had better skin permeation enhancement effect compare with GMO formulations.

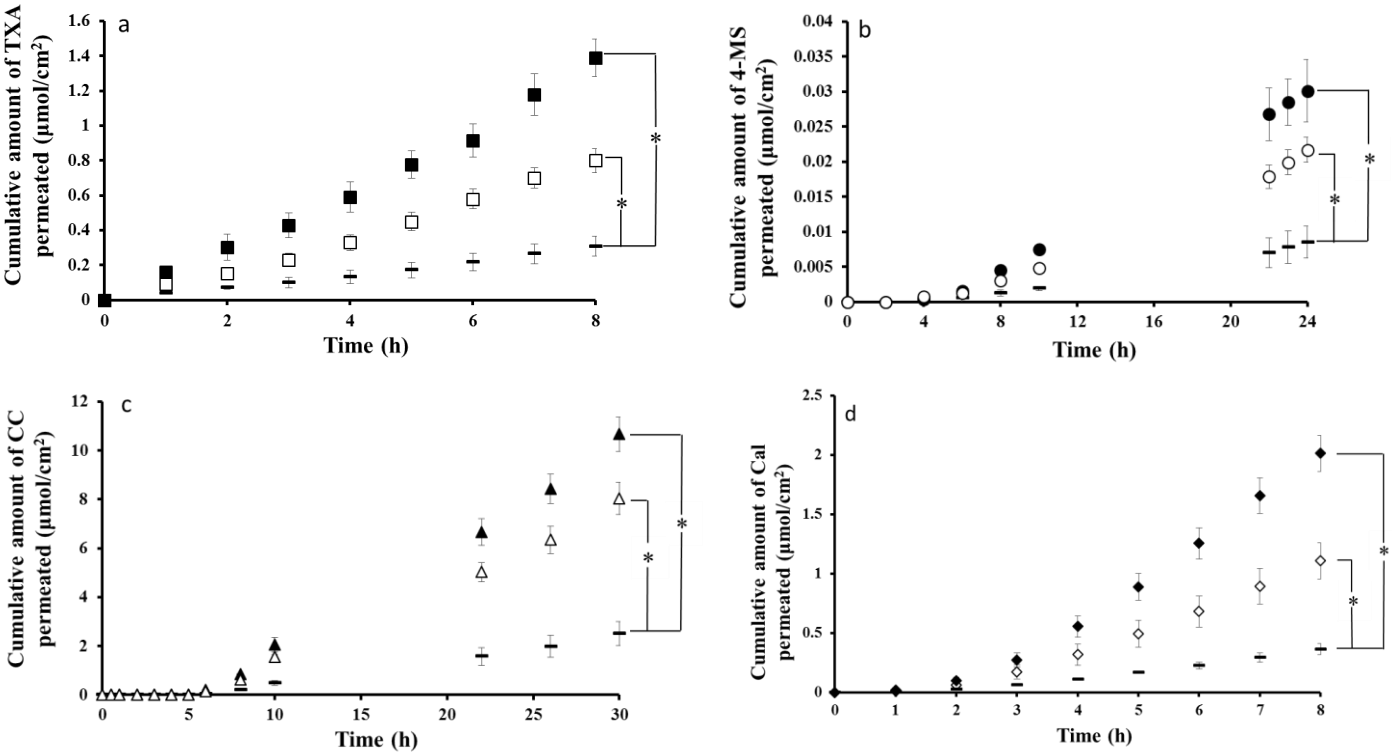

Fig. 2-7. Effect of LC formulation on the time course of the cumulative amount of TXA (a), 4-MS (b), CC (c) and Cal (d) that permeated through hairless rat intact skin.

Symbols: (a): (—), TXA solution; (■), TXA-MGE formulation; (□), TXA-GMO formulation; (b): (—), 4-MS solution; (●), 4-MS-MGE formulation; (○), 4-MS-GMO formulation; (c): (—), CC solution; (▲), CC-MGE formulation; (△) CC-GMO formulation; (d): (—), Cal solution; (◆), Cal-MGE formulation; (◇), Cal-GMO formulation. Each point represents the mean ± S.E. of three experiments. *: $P < 0.05$ significantly different from drug solution (Student's *t*-test).

2.4. Discussion

LC-forming lipids represent an important class of biocompatible amphiphiles, and their application extends to several fields, such as cosmeceutical, dietary and pharmaceutical technologies [38]. In recent years, the LC phases formed by LC-forming lipids have been shown to be able to accommodate biologically active molecules such as vitamins, enzymes and other proteins [62-64]. This ability opens new possibilities for pharmaceutical applications. Previous researches have demonstrated that the LC phases, such as cubic and hexagonal phases, increased transdermal drug delivery [4, 65]. The advantages of LC formulations for transdermal drug delivery systems might include biocompatibility and the ability to self-assemble their structure [12].

In the present study, we investigated the usefulness of MGE-LC as a new skin permeation enhancing approach, and the obtained results were compared with GMO as one of the most widely studied LC-forming lipids used in topical formulations.

TXA, 4-MS and CC drug models were selected due to their topical therapeutic beneficial. Topical application of TXA to bleeding wound surfaces can reduce the blood loss. 4-MS can be used to treat skin conditions that involve scaling or overgrowth of skin cells such as psoriasis, ichthyoses, corns, calluses and warts on the hands or feet. CC can inhibit skin tumorigenesis, reducing inflammation, protecting skin from UV-induced various damages and inhibiting formation of melanin. However, these drug models have low transdermal absorption [66, 67]. Moreover, Cal has low transdermal absorption because of its hydrophilicity and large molecular weight. Therefore, TXA, 4-MS, CC and Cal were selected as drug models for skin studies.

We prepared LC formulations using MGE and GMO containing drugs based on a 1:1 ratio, as shown in Table 2-2. These formulations were prepared by extruding lipid dispersion 50 times with a microsyringe dispenser, to incorporate high percentage of lipid (50%) with the drug solution (50%). This technique has an advantage by mixing high concentration of lipid up to 50% with the drug solution without the aid of dispersant. Non-uniform mixtures

with high viscus aggregate were observed using other techniques such as homogenizer and ultrasonic even in the presence of dispersants.

Birefringence was investigated for the prepared formulations using a polarizing light microscope. As a result, TXA-, 4-MS-, CC- and Cal-MGE and GMO formulations showed a clear optical anisotropy on the images; however, no optical anisotropy was observed in the case of MGE and GMO alone (Fig. 2-1a, b). These results strongly suggested that both MGE and GMO formulations managed to form crystalline formulations successfully because of the high birefringence of these formulations.

Furthermore, the phase structure of the formulations was examined by SAXS, and the results showed that typical reflection patterns at nearly 1, √3, and √4 for both MGE and GMO formulations revealed the presence of a hexagonal phase (H_1, H_2) (Fig. 2-3a-d) (Fig. 2-3e-h in Appendix / Supplementary data). The driving force of forming hexosome systems is the physically applied shear stress by microsyringe dispensers.

The critical packing parameter (CPP) is useful in predicting which phases can be preferentially formed by a given lipid. When CPP < 1, oil-in-water self-assembled structures form, such as normal micelles, normal cubic structure, and normal hexagonal phases. When CPP > 1, water-in-oil self-assembled structures form, such as reversed micelles, reversed cubic structure, and reversed hexagonal structure [8]. Additives or active ingredients might affect CPP as well as the LC phase structure. Generally, GMO formed the invert-type LC with CPP > 1 [58]. No previous studies have performed on the effect of CPP on the LC phase structure formed by MGE.

Previous studies have reported that the hexagonal phase presents some advantages. It has a larger surface area to interact with the skin, high fluidity, and can be incorporated into compounds independently of their solubility [68, 69]. Although a hexagonal phase (H_1, H_2) was formed in all prepared formulations, factors such as concentration of lipid and drug could influence the phase transition of these formulations. Further studies are necessary to be conducted to understand the effect of such factors on the phase transition of LC formulations.

The particle size and zeta potential of MGE- and GMO-LC formulations were determined immediately (Fig. 2-4a, b) and at 10 days after preparation (Fig. 2-4c, d in Appendix / Supplementary data). The obtained data showed that these formulations had small particle size (220-280 nm) and the zeta potential ranged between -17 and -30 mV. In addition, no significant changes were observed in the particle size or zeta potential measurements at 10 days after preparation. These results suggested that the present MGE and GMO formulations had small particle size with high surface charges and electrical repulsion between the particles, and thus their aggregation was prevented even 10 days after preparation. The zeta potential presented strong negative values for all the analyzed samples, indicating the predominance of repulsive forces. The reason why LC formulations showed negative zeta potential values is due to the present of free oleic acid in the lipid phase may give rise to the negative charge of the particles. In addition, the negative charge can also be explained by preferential adsorption of hydroxyl ions at the lipid-water interface.

These results were consistent with previous findings on the zeta optional of LC formulations [70].

Furthermore, the viscosity of the formulations was measured. The viscosity of LC formulations with MGE was significantly lower than those with GMO. In contrast to MGE, the high viscosity of GMO makes it less easy to handle, impractical for drug loading, and requires melting at 70°C before use. These results suggested that the type of LC-forming lipid dramatically affected the viscosity of the formulation (Fig. 2-5). In consequence, the drug release results showed that the low viscosity of MGE-LC-formulations could influence the drug diffusivity and the release rate of the entrapped drugs in these formulations (Fig. 2-6). In general, hydrophilic drugs are tended to be located close to the polar head of lipid or in the water channels (water phase), whereas lipophilic drugs will be loaded in the lipid bilayer and amphiphilic drugs in the interface (lipid phase). The aqueous and lipid phases in the present formulation design were in a ratio 1:1, therefore, these formulations can accommodate a wide range of different physicochemical drugs. The obtained release profiles suggest that the viscosity of hexagonal is the decisive factor mainly influenced of drug

diffusion in LC-formulations. The low viscosity of MGE could be related to the chained-liked terpenes and double bound in its structure (Fig. 1-1).

In vitro skin permeation experiment was carried out using hairless rat skin. Correlation of skin permeation of chemicals to human skin is very important and previous studies showed a good relationships of skin permeation of chemicals between human and hairless rat skin [71, 72]. Significant improvement in the skin permeation of different drugs was observed after application of MGE and GMO formulations (Fig. 2-7). The enhancement of the skin permeation ratio of MGE formulations was higher than those of GMO formulations. These results clearly showed that MGE formulations managed to improve the skin permeation enhancement effect compared with GMO formulations. These findings could be related to the low viscosity of MGE formulations, and this might offer better drug diffusivity and influence the movement and permeation of the drugs in and across the skin. The detailed mechanism of the skin permeation enhancing ability by LC systems is not fully understood [73]. It was speculated that cubic structure with similar nano-structure as the skin, increases the interaction between skin and formulation and enhances the skin permeation [74, 75]. A previous study [76] reported that the hexagonal phase may facilitate the fusion of LCs with the stratum corneum and deeper skin layers and thereby may improve drug delivery to the skin. Moreover, the hexosome system, owing to its larger surface area to interact with the skin and high fluidity, can be incorporated into compounds independently of their solubility [68, 69]. Further studies are needed to clarify the mechanism and effect of LC phase structure on the skin permeation of drugs.

2.5. Chapter conclusion

The present study confirmed that both MGE- and GMO-LC-forming lipids shared the same behavior in terms of their birefringence index, LC phase structure, particle size and zeta potential. Both the MGE- and GMO-LC formulations managed to improve skin permeation of various physicochemical properties of the drugs. However, MGE formulations had lower viscosity, faster drug release and better skin permeation than GMO formulations. The results in the second chapter strongly suggested that the low viscosity of MGE-LC-formulations might influence drug diffusivity and permeability through skin. The present MGE-LC forming lipid can be utilized as a promising new topical formulation for therapeutic drugs and cosmetic ingredients.

Chapter 3

Designing and optimizing of liquid crystal formulations for oral administration and transdermal application

3.1. Introduction

As previously stated, increasing attention has been paid to LC formulations, such as cubosomes and hexosomes, because of their remarkable structural complexity and usefulness in various pharmaceutical applications. LC-forming lipids represent an important class of biocompatible amphiphiles, and their application extends to several fields, such as cosmeceutical, dietary, and pharmaceutical technologies [38, 12]. LC phases are able to accommodate biologically active molecules such as vitamins, enzymes, and other proteins [63, 64]. The advantages of LC formulations as a drug-delivery system are their high biocompatibility and the self-assembly ability of their structure. This ability opens new possibilities for pharmaceutical applications [8]. Several studies have reported the usefulness of LC formulations to enhance the drug absorption after oral and transdermal application [57, 77]. Ali *et al*. reported enhancing effect of orally administered poorly water soluble drugs of spironolactone (estimated log $K_{octanol/water}$: 2.9 and molecular weight (MW): 417) and nifedipine (estimated log $K_{octanol/water}$: 2.2 and MW: 346) with reverse bicontinuous cubic phase of monoolein [78]. Nguyen *et al*. investigated the ability of nanostructured reverse bicontinuous cubic phase of monoolein to sustain the absorption of a poorly water soluble drug, cinnarizine (estimated log $K_{octanol/water}$: 5.8 and MW: 369) after oral administration [28]. In addition, Cohen-Avrahami *et al*. examined skin permeation-enhancement effect of a hydrophilic drug, sodium diclofenac (log $K_{octanol/water}$: -0.1 and MW: 318) with reversed hexagonal lyotropic LC containing a skin permeation enhancer [79]. Lopes *et al*. investigated transdermal delivery of cyclosporin A (log $K_{octanol/water}$: 2.92 and MW: 1202) with reverse cubic and hexagonal phase of monoolein and also reported another successful application with the combination of vitamin K (estimated log $K_{octanol/water}$: 11.7 and MW: 451) and hexagonal phase of monoolein [65]. Furthermore, in previous studies from our laboratory

[61, 4], successful improvement was demonstrated in the drug absorption after oral and transdermal application with LC formulations that composed with MGE (Fig. 1-1), and the enhancement effect of these formulations was dramatically affected by the type of LC-forming lipids. MGE was easy-to-handle due to its low viscosity at 25 °C compared to GMO and PHT and showed better drug absorption enhancement effects. However, no studies have investigated the effect of several factors such as physicochemical properties of the entrapped drugs and concentration of LC-forming lipids and LC phase structure on the enhancement effect of orally and topically administered drugs. Therefore, in the present study, MGE was selected as an LC-forming lipid. PABA and its prodrugs, methyl *p*-aminobenzoate (M-PABA) and ethyl *p*-aminobenzoate (E-PABA) (Table 3-1) were selected as drug models with different lipophilicities to understand the effect of the lipophilicity changes on the drug absorption performance of LC formulations. On the other hand, for transdermal LC formulations, only hydrophilic sodium fluorescein (Na-FL) was selected as a model drug and was entrapped with different concentrations of MGE. Overcoming the stratum corneum barrier to cutaneously deliver hydrophilic drugs is one of the major challenges in the field of dermatologic therapy; therefore, Na-FL was used as a well-known hydrophilic and mal-absorbed model drug in this study. Thus, in the present study I aimed to develop strategies for designing and optimizing oral and topical LC formulations by evaluating the effect of these factors on the drug absorption from LC formulations.

Table 3-1 Physicochemical properties of the compounds used in the present study.

	Abbreviation	M.W.	ClogP
p-Amino benzoic acid	PABA	137.14	0.98
Methyl *p*-aminobenzoate	M-PABA	151.17	1.39
Ethyl *p*-aminobenzoate	E-PABA	165.19	1.93
Sodium fluorescein	Na-FL	376.27	-2.02

3.2. Materials and methods

3.2.1. Materials

MGE (purity: > 99.56%) was obtained from Farnex Co., Inc. (Yokohama, Japan). PABA, M-PABA and E-PABA were purchased from Kanto Chemical Co., Inc. (Tokyo, Japan). Na-FL was purchased from Tokyo Chemical Industry Co., Ltd. (Tokyo, Japan). A surfactant, Pluronic® F127, was purchased from Sigma-Aldrich (St. Louis, MO, USA). Other reagents and solvents were of special grade or HPLC grade and used without further purification.

3.2.2. Preparation of oral and topical LC formulations

Table 3-2 lists the oral and topical LC formulations used in this study. These formulations were designed based on changing the concentration of MGE in the formulations and entrapped with drugs with different physicochemical properties. The mixture was dispersed using a homogenizer (Polytron PT-MR 3000; Kinematica Inc., Littau, Switzerland). The dry powder LC formulations were prepared using a freeze dryer (Labcono FZ-18; Asahi Life Science Co. Ltd., Tokorozawa, Saitama, Japan).

Table 3-2 Composition of oral and topical LC formulations.

Formulation code	Composition of oral LC formulations
OP5*	PABA solution containing 5% Pluronic® F127 and 5% MGE
OP10	PABA solution containing 5% Pluronic® F127 and 10% MGE
OP20	PABA solution containing 5% Pluronic® F127 and 20% MGE
OP30*	PABA solution containing 5% Pluronic® F127 and 30% MGE
OP10D	PABA dry powder formulation containing 5% Pluronic® F127, 10% MGE, 10% mannitol and 1% ethanol
OP20D*	PABA dry powder formulation containing 5% Pluronic® F127, 20% MGE, 10% mannitol and 1% ethanol
OM5*	M-PABA solution containing 5% Pluronic® F127 and 5% MGE
OM10	M-PABA solution containing 5% Pluronic® F127 and 10% MGE
OM20	M-PABA solution containing 5% Pluronic® F127 and 20% MGE
OM30*	M-PABA solution containing 5% Pluronic® F127 and 30% MGE
OM10D	M-PABA dry powder formulation containing 5% Pluronic® F127, 10% MGE, 10% mannitol and 1% ethanol
OM20D*	PABA dry powder formulation containing 5% Pluronic® F127, 20% MGE, 10% mannitol and 1% ethanol
OE5*	E-PABA solution containing 5% Pluronic® F127 and 5% MGE
OE10	E-PABA solution containing 5% Pluronic® F127 and 10% MGE
OE20	E-PABA solution containing 5% Pluronic® F127 and 20% MGE
OE30*	E-PABA solution containing 5% Pluronic® F127 and 30% MGE
OE10D	E-PABA dry powder formulation containing 1% Pluronic® F127, 10% MGE, 10% mannitol and 1% ethanol
OE20D*	M-PABA dry powder formulation containing 5% Pluronic® F127, 20% MGE, 10% mannitol and 1% ethanol
TF5**	Na-FL solution containing 5% Pluronic® F127 and 5% MGE
TF10	Na-FL solution containing 5% Pluronic® F127 and 10% MGE
TF20	Na-FL solution containing 5% Pluronic® F127 and 20% MGE
TF30	Na-FL solution containing 5% Pluronic® F127 and 30% MGE
TF40	Na-FL solution containing 5% Pluronic® F127 and 40% MGE
TF50**	Na-FL solution containing 5% Pluronic® F127 and 50% MGE

The concentration of PABA, M-PABA, or E-PABA in the formulation was 10 mM and the concentration of Na-FL was 5 mM.

Formulation code: O = Oral formulation; T = Topical formulation; P = PABA; M = M-PABA; E = E-PABA; F = Na-FL; D = Dry powder; Number = Percentage of MGE.

*: Rejected oral formulations.

**: Rejected topical formulations.

3.2.3. Measurement of particle size and zeta potential

The particle size and zeta potential of LC formulations were determined using a dynamic light scattering Nano-ZS ZEN3600 Zetasizer (Malvern Instruments Ltd., Worcestershire, U.K.). LC samples were diluted in distilled water and shaken using a vortex mixer prior to measurement.

3.2.4. SAXS measurement

SAXS measurement of dispersed formulations was performed using a Nano-Viewer (Rigaku, Tokyo, Japan) with a Pilatus 100K/RL 2D detector. The X-ray source was Cu Kα radiation with a wavelength of 1.54 Å and operating at 45 kV and 110 mA. The sample-to-detector distance was set at 375 mm. Each sample was placed into a vacuum-resistant glass capillary cell and exposed at 25°C for 10 min. The SAXS pattern obtained was plotted against the scattering vector length, $q = (4\pi/\lambda)\sin(\theta/2)$, where θ is the scattering angle.

3.2.5. Release experiment

A dialysis membrane (molecular weight cut-off; 2,000–14,000 Da, Sanko Junyaku Co., Tokyo, Japan) was set in a vertical-type diffusion cell (effective diffusion area: 0.95 cm^2) and the receiver chamber was maintained at 32°C. Phosphate-buffered saline (PBS; pH 7.4) was applied to the receiver chamber. Drug (PABA, M-PABA, E-PABA or Na-FL) solution (1.0 mL) or its LC formulation (1.0 mL) was applied to the donor cell to start the release experiment. An aliquot (500 μL) was withdrawn from the receiver chamber, and the same volume of PBS was added to the chamber to keep the volume constant. The amount of PABA, M-PABA, and E-PABA released was determined using an HPLC (Shimadzu Ltd., Kyoto, Japan). In case of Na-FL, the released amount was determined using a fluorescence spectrophotometer (Shimadzu Ltd., Kyoto, Japan). The cumulative % of drug released was plotted against the square root of time (Higuchi's plot) [29].

3.2.6. Animals

Male hairless (WBM/ILA-Ht) and male Wistar (Slc) rats were purchased either from Life Science Research Center, Josai University (Sakado, Saitama, Japan) or Ishikawa Experiment Animal Laboratories (Fukaya, Saitama, Japan). Animals were housed in temperature-controlled rooms (25 ± 2°C) with a 12 h light-dark cycle (07:00–19:00 h). The rats were allowed free access to food (Oriental Yeast Co., Tokyo, Japan) and tap water. The animal experiment protocol was approved by the Animal Care and Use Committee of Josai University (Sakado, Saitama, Japan).

3.2.7. HPLC conditions

The *in vivo* or *in vitro* study sample (50 µL) was mixed with the same volume of acetonitrile containing methyl paraben (10 µg/mL) as an internal standard and centrifuged (5 min, 4°C). The obtained supernatant (20 µL) was injected into an HPLC system (Shimadzu, Kyoto, Japan), which consisted of a system controller (CBM-20A), pump (LC-20AD), auto-sampler (SIL-20AC), column oven (CTO-20A), UV detector (SPD-M20A) and analysis software (LC Solution). The column was an GL Sciences Inc. ODS-3 (5 µm, 4.6 × 250 mm) (Nihon Waters K.K., Tokyo, Japan), which was maintained at 40°C. The mobile phase was acetonitrile : 0.1% phosphoric acid = 8 : 52 (0–4 min), 35 : 65 (4–14 min) and 8 : 92 (14–20 min). The flow rate was adjusted to 1.0 mL/min. PABA, M-PABA and E-PABA were detected at UV 280 nm.

3.2.8. Determination of bioavailability

Intravenous and oral administrations were performed in Wistar rats under anesthesia by intraperitoneal injection of three types of anesthesia (medetomidine, 0.375 mg/kg; butorphanol, 2.5 mg/kg; and midazolam, 2 mg/kg) to determine the bioavailability of PABA. In case of intravenous administration, PABA dissolved in physiological saline (PABA solution) was injected (5.0 µmol/kg) into the tail vein. Blood samples (0.2 mL) were collected from the jugular vein at predetermined intervals up to 3 h, and the same volume of saline was injected via the tail vein to prevent severe changes in the volume of distribution. For oral

administration, PABA solution or LC-formulation (10 μmol/kg) was administered to rats, and blood (0.2 mL) was withdrawn from the jugular vein at intervals up to 6 h and the same volume of saline was injected via tail vein. Blood samples placed into heparinized tubes were immediately separated by centrifugation to obtain plasma (5 min, 4°C). Plasma and skin samples were stored at -30°C until analysis.

3.2.9. *In vitro* skin permeation experiment

Full-thickness hairless rat skin was excised from the abdomen under anesthesia by *i.p.* injection of three types of anesthesia as above. Excess fat was trimmed off, and the skin samples were set in vertical-type diffusion cells with the epidermis side facing the donor compartment. PBS was applied to the receiver chamber as in the release experiment and maintained at 32°C. These skin permeation experiments were conducted after hydration for 60 min with PBS. Drug solution (1.0 mL) or its LC-formulation (1.0 mL) was applied to the donor cell to start the *in vitro* skin permeation experiment. An aliquot (500 μL) was withdrawn from the receiver chamber, and the same volume of PBS was added to the chamber to keep the volume constant. The skin permeation of Na-FL was determined using a fluorescence spectrophotometer.

3.2.10. Determination of *AUC*

The area under the plasma concentration–time curve (*AUC*) was calculated using the linear trapezoidal rule. The absolute bioavailability was determined as AUC_{po}/AUC_{iv} using the mean *AUC* values for oral and intravenous doses.

3.2.11. Statistical analysis

Statistical analysis was performed using unpaired Student's *t*-test (ANOVA), and *P* values less than 0.05 were considered to be significant.

3.3. Results

3.3.1. Homogeneity and visible appearance

First, the homogeneity and visible appearance of the prepared LC formulations were evaluated. Accepted formulations were a uniform opaque white mixture or uniform powder without visible signs of aggregates, whereas rejected formulations appeared as a non-uniform dispersion or aggregated wet powder. Figure 3-1 shows photographs to illustrate these criteria for accepted and rejected formulations. OP30, OM30, and OE30 (Table 3-2) were inconvenient for oral due administration because of the high percentage of lipid (creamy formulations); therefore, these formulations were not studied for oral administration. However, these formulations were accepted for topical application (TF30 and TF40) (Table 3-2). Non-uniform mixtures with aggregates were observed with a high percentage of LC-forming lipid (> 40%); therefore, no further work was carried out with these formulations. Fine powders were obtained in OP10D, OM10D, and OE10D (Table 3-2). However, when the MGE content increased to 20% (OP20D, OM20D, and OE20D, respectively) (Table 3-2), aggregated wet powders were observed. Therefore, no further work was carried out with them.

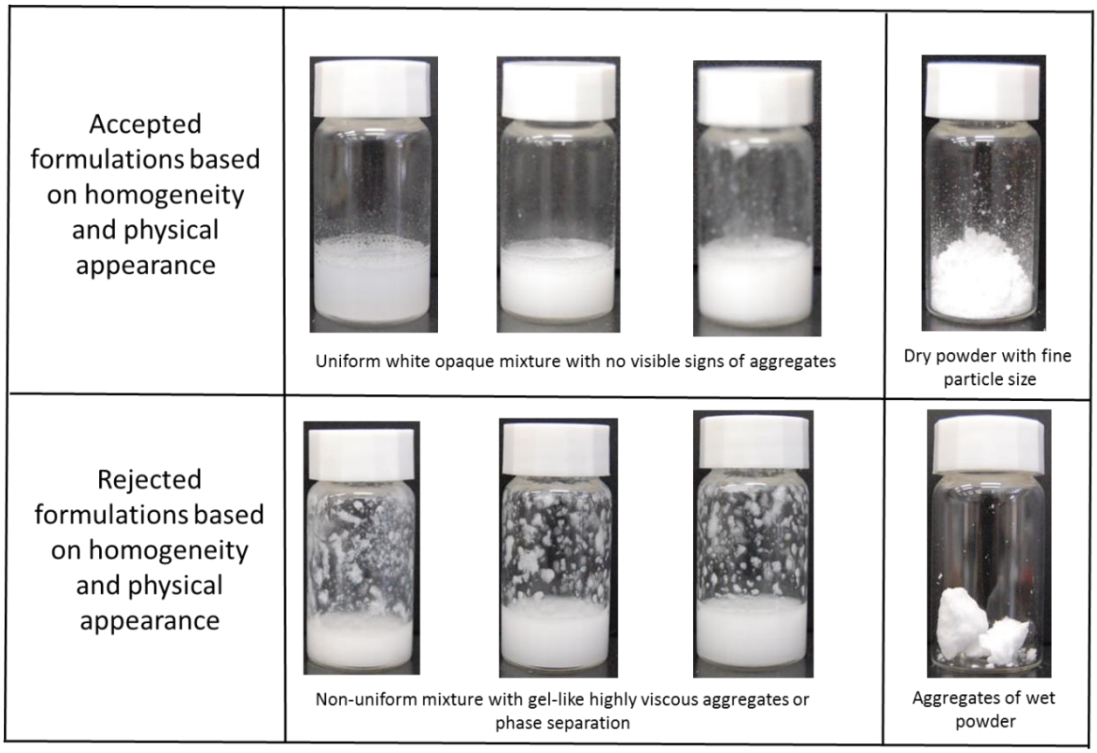

Fig. 3-1. Illustration photographs of accepted and rejected LC formulations based on homogeneity and visible appearance. Accepted formulations were appeared as a uniform opaque white mixture or uniform powder without visible signs of aggregates, while rejected formulations were appeared as a non-uniform dispersion or aggregated wet powder.

3.3.2. Particle size and zeta potential measurement

Table 3-3 shows particle size and zeta potential values of oral and topical LC formulations. The obtained results showed that the particle size tended to be smaller and the zeta potential became more negative with increasing MGE content. Formulations with low MGE content represented by 5% (*i.e.*, OP5, OM5, OE5, and TF5) tended to have large particle size and low negative surface charge. Because the low surface charge indicated low stability of the 5% MGE formulations, no further work was carried out with these formulations.

Table 3-3 Particle size (nm) and zeta potential (mV) of LC formulations.

Formulation code	Particle size (nm)	Zeta potential (mV)
OP5	409 ± 26	-3.1 ± -0.8
OP10	340 ± 21	-10.4 ± -1.7
OP20	288 ± 17	-15.5 ± -2.3
OP10D	366 ± 27	-10.7 ± -1.4
OM5	488 ± 23	-2.8 ± -0.7
OM10	327 ± 14	-11.7 ± -1.3
OM20	301 ± 29	-16.2 ± -2.4
OM10D	332 ± 27	-6.9 ± -1.1
OE5	412 ± 31	-2.6 ± -0.6
OE10	384 ± 28	-12.4 ± -1.8
OE20	311 ± 18	-17.6 ± -2
OE10D	377 ± 27	-7.9 ± -1.2
TF5	388 ± 22	-3.1 ± -0.7
TF10	348 ± 12	-12.1 ± -1.5
TF20	328 ± 26	-17.4 ± -1.3
TF30	351 ± 21	-22.7 ± -3.4
TF40	311 ± 17	-30.4 ± -4.2

Each value represents the mean ± S.E. of 3 experiments.

3.3.3. Drug release properties from LC formulations

Figure 3-2a-d show the release profile of PABA, M-PABA, E-PABA and Na-FL, respectively, from their LC formulations. All profiles obeyed the Higuchi's law [29]: high correlation coefficients ($r > 0.99$) were obtained for each formulation, indicating that *in vitro* drug release profiles of drug were well fitted with the square root Higuchi model.

For oral formulations, the amounts of PABA released from OP10D, OP10, OP20 and OP30 were 13.9 ± 2.5%, 23.7 ± 3.2%, 16.7 ± 2.8% and 9.6 ± 0.8% (Fig. 3-2a), respectively, against the initial dosing. Those of M-PABA from OM10D, OM10, OM20, and OM30 were 6.4 ± 0.4%, 5.7 ± 0.3%, 4.2 ± 0.2% and 3.4 ± 0.4% (Fig. 3-2b), respectively, and those of E-PABA from OM10D, OM10, OM20 and OM30 were 3.8 ± 0.3%, 3.4 ± 0.3%, 2.5 ± 0.2%, and 2.2 ± 0.2% (Fig. 3-2c), respectively. For topical formulations, the amounts of Na-FL released from TF10, TF20, TF30 and TF40 were 18 ± 0.6%, 15.5 ± 0.7%, 11.5 ± 0.6% and 6.0 ± 0.7% (Fig. 3-2d), respectively.

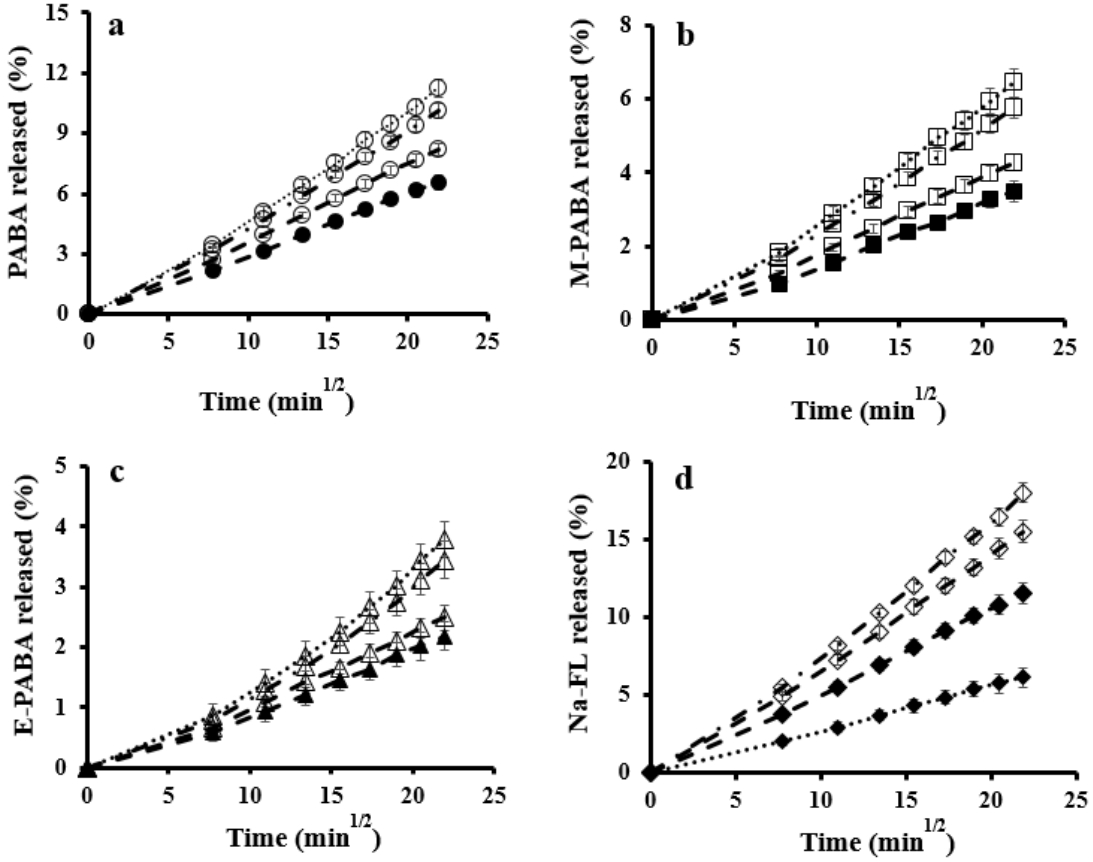

Fig. 3-2. Effect of LC forming lipid concentration and physicochemical properties of entrapped drug on the release profile of PABA (a), M-PABA (b), E-PABA (c) and Na-FL (d) from their LC formulations. Symbols: (a): (○⋯), OP10D formulation; (○-·-·), OP10 formulation; (○---), OP20 formulation; (●---), OP30 formulation; (b): (□⋯), OM10D formulation; (□-·-·), OM10 formulation; (□---), OM20 formulation; (■---), OM30 formulation; (c): (△⋯), OE10D formulation; (△-·-·), OE10 formulation; (△---), OE20 formulation; (▲---), OE30 formulation; (d): (◇-·-·), TF10 formulation; (◇---), TF20 formulation; (◆---), TF30 formulation; (◆⋯), TF40 formulation. Each point represents the mean ± S.E. of three experiments.

Although the release profile was influenced by changes in the MGE concentration, it was influenced more dramatically by changes in the physicochemical properties of the entrapped drugs. For example, the release amount of Na-FL from TF10 was 18 ± 0.6% (Fig. 3-2d) as compared with the release of E-PABA from OE10, 3.8 ± 0.3% (Fig. 3-2c), although both formulations contained the same concentration of MGE.

3.3.4. SAXS chart of LC formulations

The phase structure of LC formulations was evaluated by SAXS. Figure 3-3a-c shows the X-ray diffraction profiles of OP10 (Fig. 3-3a), OP20 (Fig. 3-3b) and OM10 (Fig. 3-3c) formulations. Typical peaks reflection distance ratios at nearly 1, √3 and √4, revealed the presence of an H_2 inverted hexagonal phase. The same peaks reflection distance ratios were observed for OM20, OE10, OE20, TF10, TF20, TF30 and TF40 (data not shown). The phase behavior of these formulations was determined based on international tables for crystallography [30, 31]. Unidentified peaks were observed for oral dry powder LC formulations OP10D (Fig. 3-3d), OM10D (Fig. 3-3e) and OE10D (Fig. 3-3f).

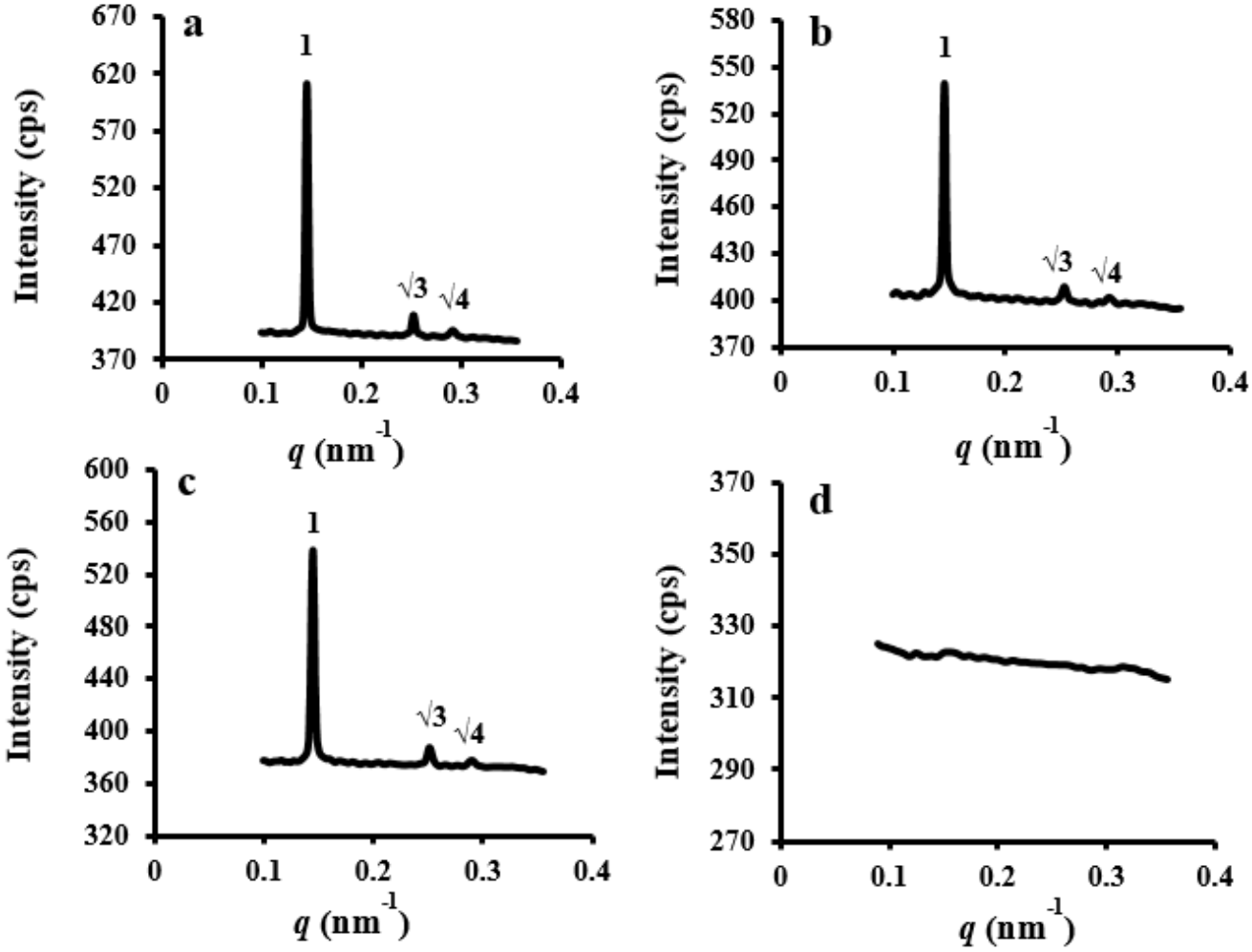
a
1
√3
√4
Intensity (cps)
670
620
570
520
470
420
370
0
0.1
0.2
0.3
0.4
q (nm-1)
b
1
√3
√4
Intensity (cps)
580
550
520
490
460
430
400
370
0
0.1
0.2
0.3
0.4
q (nm-1)
c
1
√3
√4
Intensity (cps)
600
560
520
480
440
400
360
320
0
0.1
0.2
0.3
0.4
q (nm-1)
d
Intensity (cps)
370
350
330
310
290
270
0
0.1
0.2
0.3
0.4
q (nm-1)

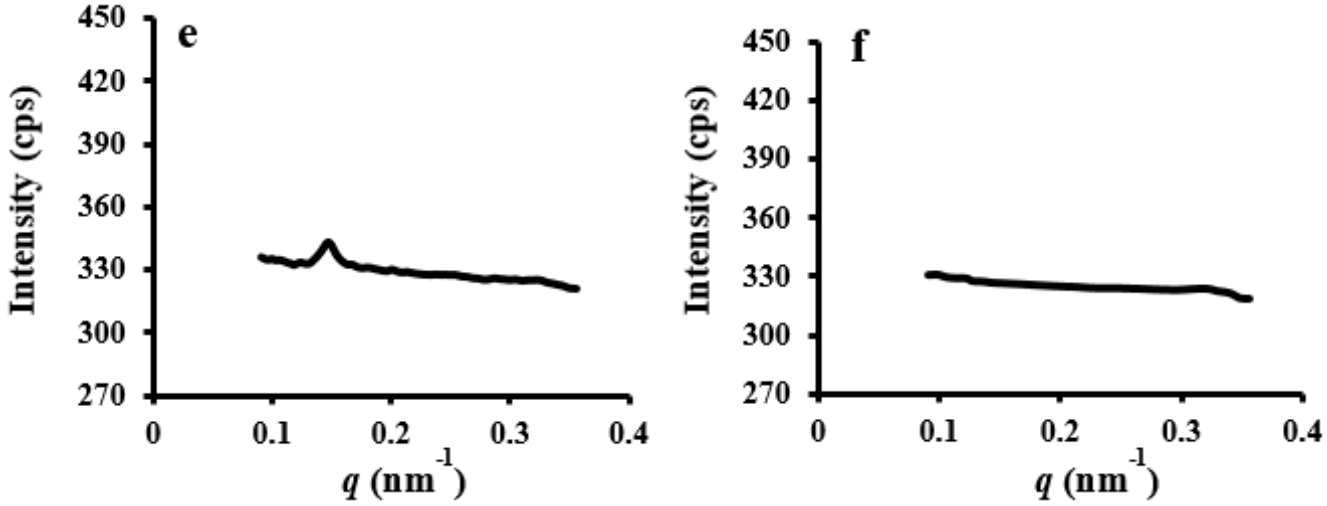

Fig. 3-3. SAXS charts of LC formulations: (a), OP10 formulation; (b), OP20 formulation; (c), OM10 formulation; (d), OP10D formulation; (e), OM10D formulation and (f), OE10D formulation. The peaks reflection distance ratios at: 1, √3, √4 confirm the presence of H_2 inverted hexagonal phase (a-c). The same peaks reflection distance ratios were observed for OM20, OE10, OE20, TF10, TF20, TF30 and TF40 (data were not shown). Unidentified peaks were observed for dry powder LC formulations (d-f).

3.3.5. Bioavailability of PABA

Figure 3-4 shows the time course of the plasma concentration of PABA after oral administration of its solution or PABA-, M-PABA-, and E-PABA-LC formulations in male Wistar rats. Table 3-4 summarizes the calculated $AUC_{0\text{-}6\ h}$, T_{max}, C_{max}, and absolute bioavailability (F) of PABA after oral administration.

The bioavailability after oral administration of OP20 (55 ± 13) (Fig. 3-5a), OM10 (44 ± 9) (Fig. 3-5b), and OE10 (43 ± 6) (Fig. 3-5c) was significantly higher than that of PABA solution (16 ± 2). No improvement was observed in the bioavailability for other LC formulations. The T_{max} of OP20 was faster compared with OM10 and OE10. The T_{max} of OE10 was delayed to 120 min. Only OP20, OM10, and OE10 showed significant improvement in the bioavailability of PABA. M-PABA, and E-PABA prodrugs after oral administration.

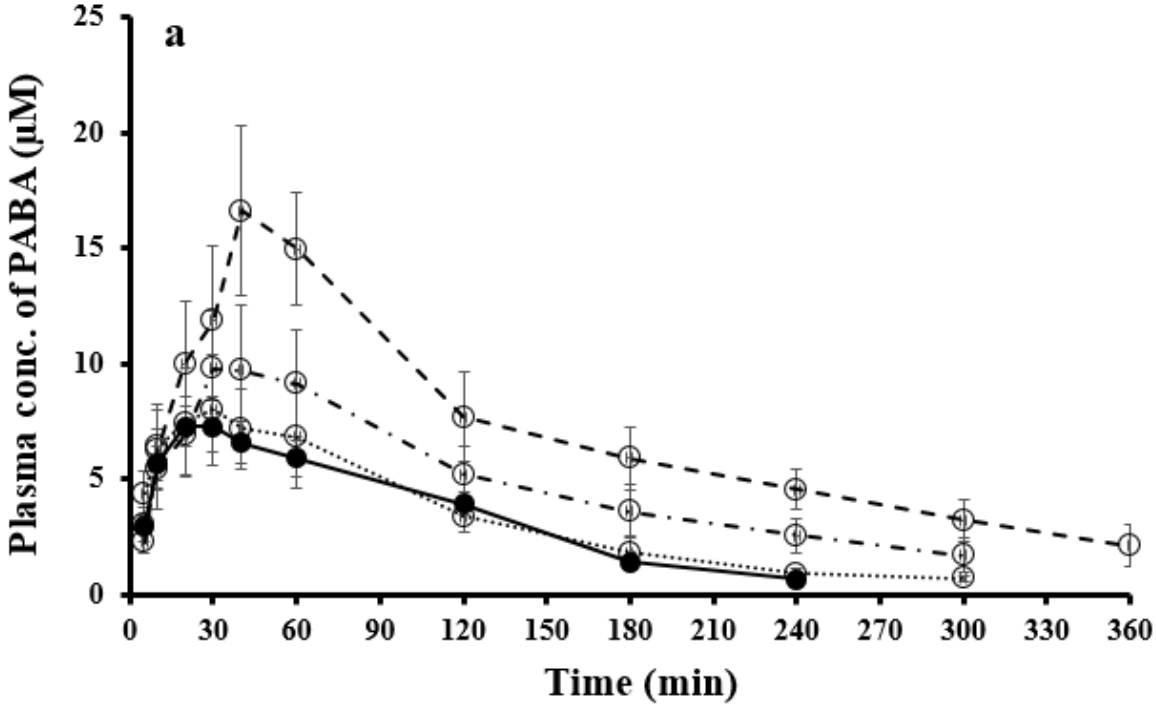
a
Plasma conc. of PABA (µM)
25
20
15
10
5
0
0
30
60
90
120
150
180
210
240
270
300
330
360
Time (min)

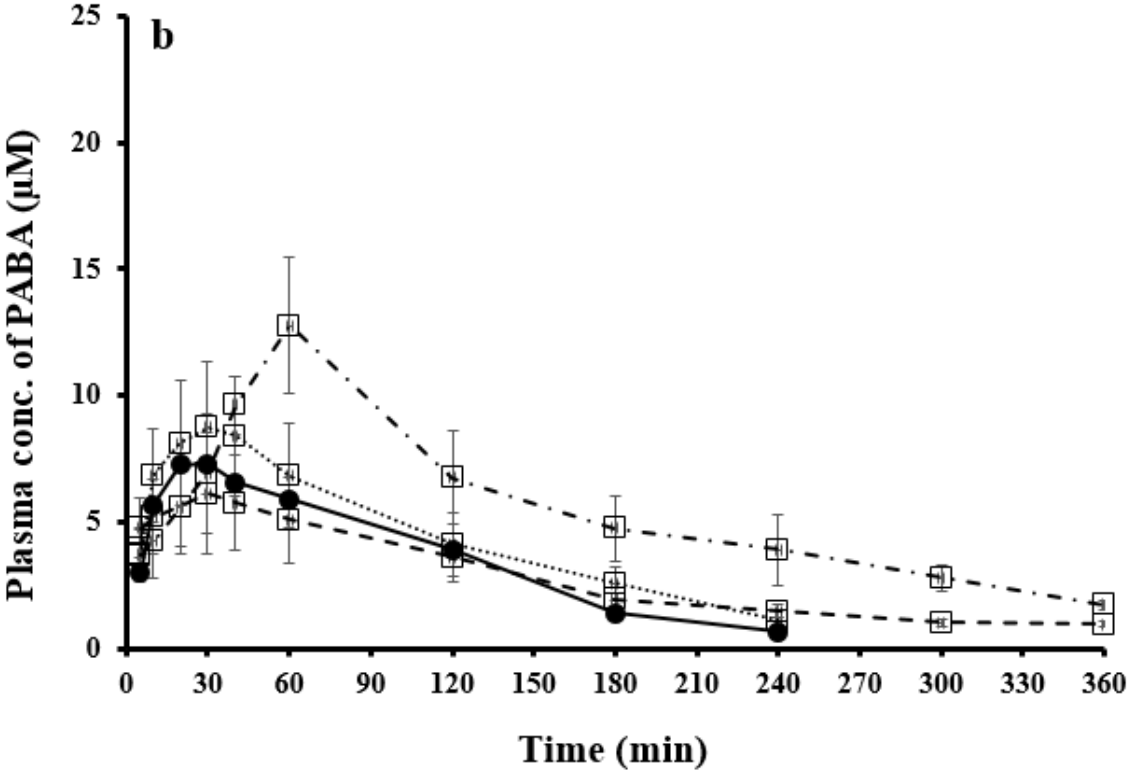
b
Plasma conc. of PABA (µM)
25
20
15
10
5
0
0
30
60
90
120
150
180
210
240
270
300
330
360
Time (min)

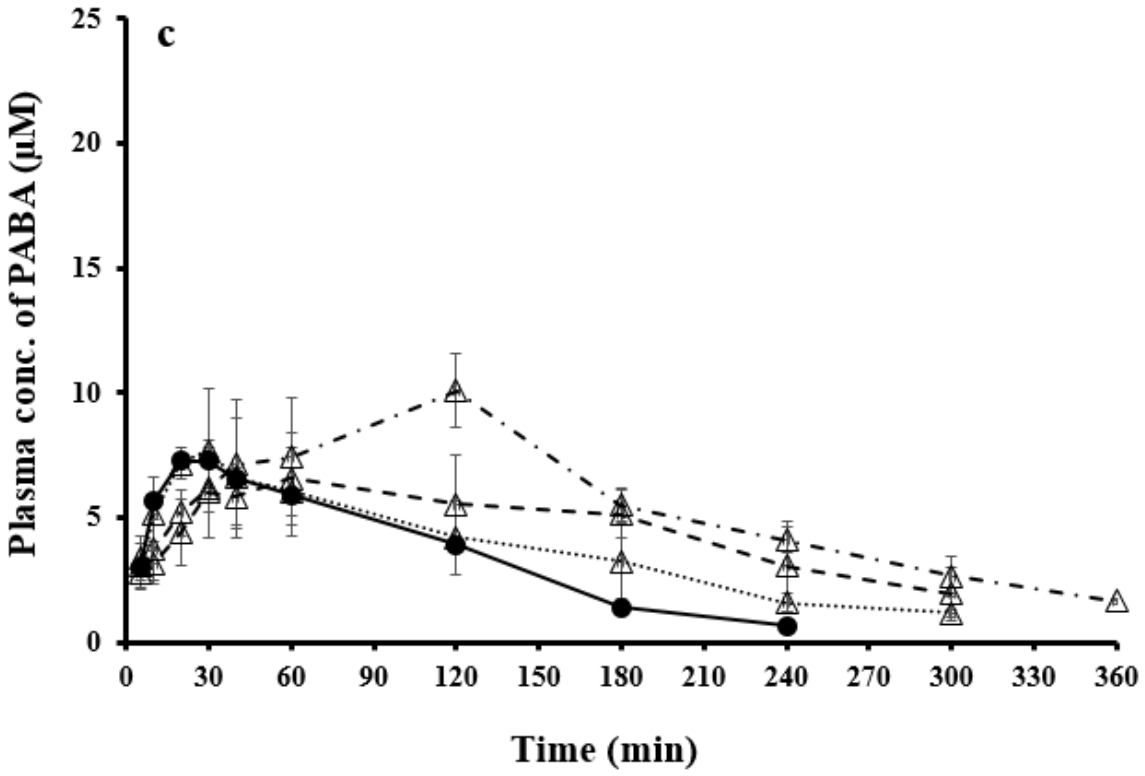

Fig. 3-4. Plasma profiles after oral administration of: (a), PABA-LC formulations; (b), M-PABA-LC formulations and (c), E-PABA-LC formulations. M-PABA and E-PABA were metabolized to PABA after oral administration. Symbols: (a): (○⋯), OP10D formulation; (○-·-·), OP10 formulation; (○---), OP20 formulation; (●—), PABA solution; (b): (□⋯), OM10D formulation; (□-·-·), OM10 formulation; (□---), OM20 formulation; (c): (△⋯), OE10D formulation; (△-·-·), OE10 formulation; (△---), OE20 formulation. Each point represents the mean ± S.E. of three experiments.

Table 3-4 Bioavailability of PABA after oral administration.

	$AUC_{0\text{-}6\ h}$	T_{max} (min)	C_{max} (μM)	MRT (min)	$F_{0\text{-}6\ h}$ (%)
PABA solution	876 ± 109	27 ± 6	7.4 ± 0.9	11 ± 1.8	16 ± 2
OP10	1595 ± 440	37 ± 6	10 ± 2.7	12.7 ± 2	30 ± 8
OP20	2939 ± 700*	46 ± 11	16 ± 3	15 ± 2.5	55 ± 13*
OP10D	1047 ± 260	33 ± 6	8 ± 2	11.4 ± 1	19 ± 4
OM10	2366 ± 496*	53 ± 11	12 ± 2.5	14 ± 2.1	44 ± 9*
OM20	1167 ± 261	33 ± 6	6 ± 2	11.8 ± 2	21 ± 5
OM10D	1072 ± 295	33 ± 6	8.8 ± 2.6	11.5 ± 2	20 ± 5
OE10	2314 ± 348*	120 ± 21	10 ± 1.5	13 ± 2.5	43 ± 6*
OE20	1519 ± 516	53 ± 11	6.5 ± 1.8	12.3 ± 3	28 ± 9
OE10D	1208 ± 348	23 ± 6	7.8 ± 2	12.1 ± 1	26 ± 6

Each value shows the mean ± S.E. of 3 experiments.

AUC: Area under the plasma concentration-time curve.
T_{max}: Time to reach the maximum plasma concentration.
C_{max}: Maximum plasma concentration.
MRT: Mean residence time.
F: Absolute bioavailability (AUC_{po}/AUC_{iv}).
*: Significantly different from PABA solution $P < 0.05$ (Student's *t*-test).

3.3.6. *In vitro* skin permeation profiles

Figure 3-5 shows the effect of LC formulations on the time course of the cumulative amount of Na-FL that permeated through hairless rat intact skin. Significant improvements in skin permeation of Na-FL were observed after application of TF20 and TF30 compared with that from the Na-FL solution. The enhancement ratios in the skin permeation for TF10, TF20, and TF30 formulations were 1.7, 4.3 and 2.9, respectively, but no improvement in skin permeation of the Na-FL was observed with TF40 formulation.

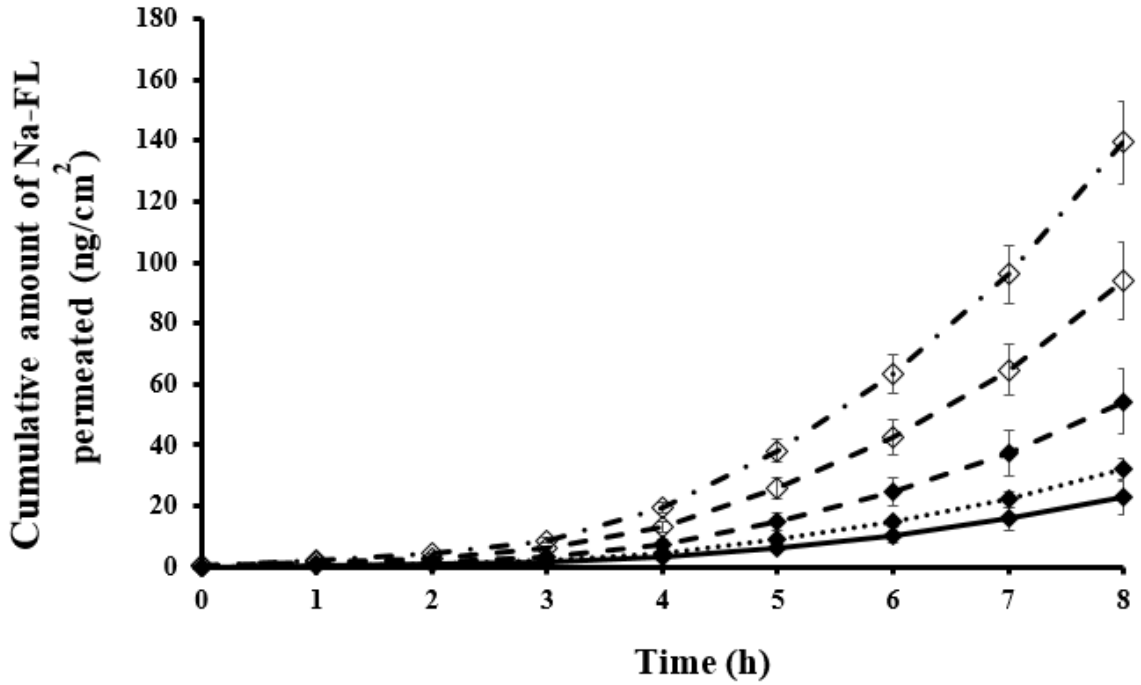

Fig. 3-5. Effect of LC forming lipid concentration on the time course of the cumulative amount of Na-FL. Symbols: (◆---), TF10 formulation; (◇-·-·), TF20 formulation; (◇---), TF30 formulation; (◆···), TF40 formulation; (◆—), Na-FL solution. Each point represents the mean ± S.E. of three experiments.

3.4. Discussion

Although LC formulations have received considerable attention because of their excellent potential as drug delivery systems [8], there seems to be a general lack of understanding among researchers regarding the effect of several factors such as physicochemical properties of the entrapped drugs, concentration of LC-forming lipids and LC phase structure on the oral and topical performance of these formulations. Therefore, the present study mainly focused on the developing strategies of oral and topical LC formulations by investigating the effect of such factors to improve the performance of these formulations.

MGE was selected as an LC forming lipid because of its low viscosity, stability and better drug absorption enhancer compared with other LC forming lipids [61]. I initially screened various oral and topical LC formulations (Table 3-2). The obtained results on their homogeneity and visible appearance (Fig. 3-1) showed that it was not recommended to prepare oral LC dispersions with MGE at a concentration of more than 30%, because these formulations tended to be too viscous and inconvenient for oral administration. When the concentration of MGE was above 40%, LC was aggregated with phase separation, therefore, they were inconvenient for both oral and topical formulations. In addition, MGE was not recommended to prepare LC dry powder at a concentration of 20% or above.

Zeta potential is an important parameter for the evaluation of stability and bio-distribution [40, 80]. By increasing the MGE concentration, the particle size tended to be smaller and the zeta potential became more negative (Table 3-3), suggesting that the number of LC forming particles was increased with an increase in the MGE concentration. The negative zeta potential of LC formulations was due to the present of free oleic acid in the lipid phase. The negative charge can also be explained by preferential adsorption of hydroxyl ions at the lipid-water interface.

As demonstrated in Fig. 3-2, the drug release profiles from LC formulations were influenced by the concentration of MGE and the physicochemical properties of the entrapped drugs. These results indicated that the drug diffusivity in the formulation decreased with an increase in MGE concentration. The drug diffusivity was affected more dramatically by changes in the physicochemical properties of entrapped drugs. The released amount of Na-

FL from TF10 was 18 ± 0.6% compared with the release of E-PABA from OE10 (3.8 ± 0.3%), although both formulations contained the same concentration of MGE (Fig. 3-2a-d). A similar phenomenon was observed with other drugs (PABA and M-PABA), and drug release decreased with an increase in lipophilicity. Figure 3-6 schematically explains the effect of lipid concentration and the physicochemical properties of entrapped drugs on drug release.

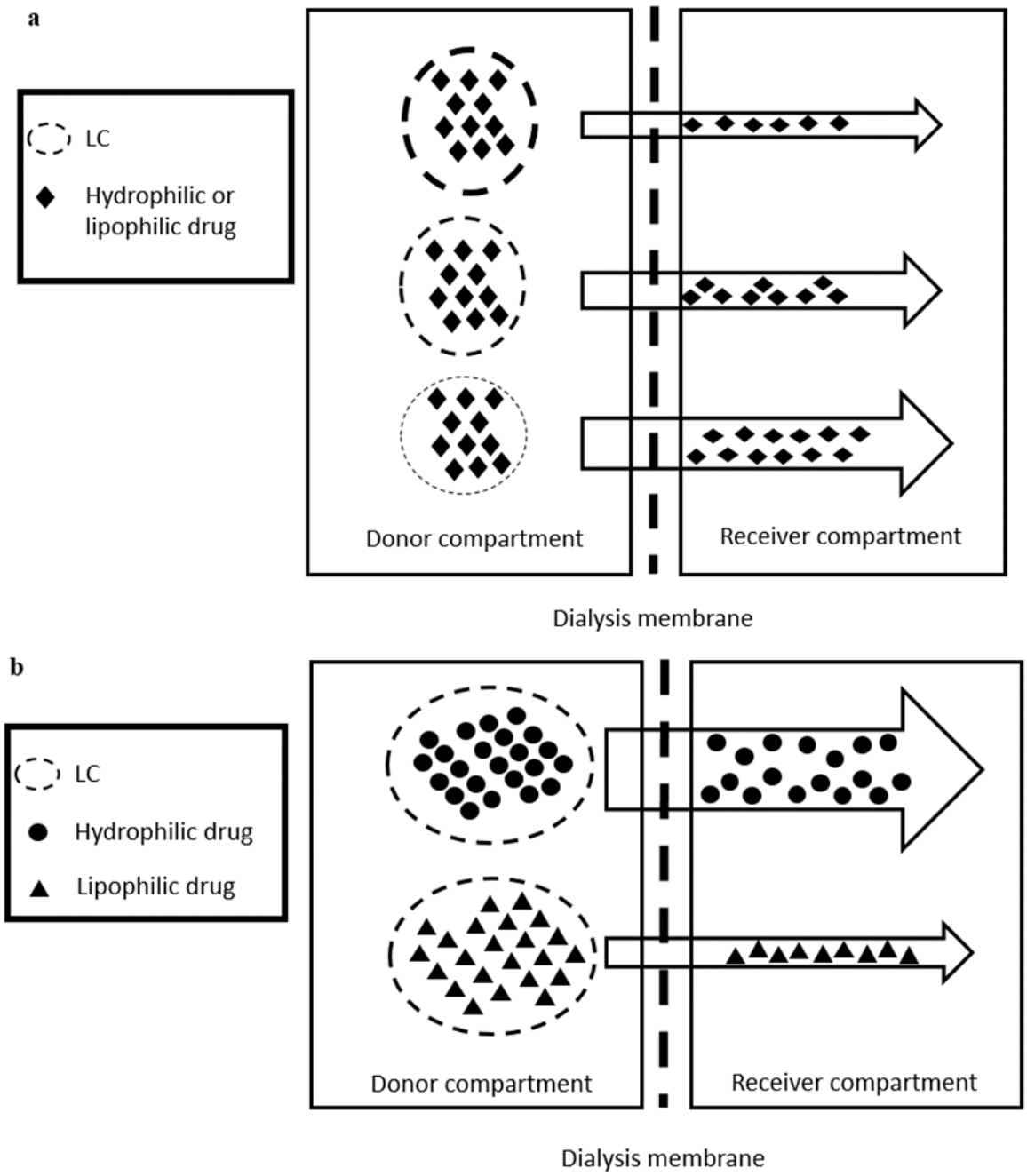

Fig. 3-6. Illustrations explaining the effect of LC concentration (a) and the physicochemical properties of entrapped drug (b) on the drug release amount. The release amount of drug is increased by a decrease of LC concentration (a). The release amount of drug is more dramatically increased by a decrease of the drug lipophilicity (b).

Typical reflection patterns at nearly 1, √3, and √4 for oral dispersions and topical LC formulations indicated that these formulations successfully managed to form an H_2 inverted hexagonal phase (Fig. 3-3a-e). Previous studies [68, 69] have reported that the hexagonal phase has several advantages. It has a larger surface area to interact with biological membranes with high fluidity, and greater amounts of drugs can be incorporated independent of their solubility. In contrast to our findings, other studies have demonstrated the presence of cubosomes using different types of LC-forming lipids such as GMO or PHT [28, 68]. I strongly believed that several factors might affect the phase structure of LC formulations, such as temperature, type of LC-forming lipid, physicochemical properties of the entrapped drugs, lipid concentration and type of surfactant. Further studies are necessary to fully understand the effect of such factors on the phase transition of LC formulations. The key point is to successfully prepare hexosomes or cubosomes by designing with LC formulations. No clear mechanism or clear evidence has been proposed to indicate that cubosomes have more potential than hexosomes, or vice versa, as a drug delivery system. On the other hand, unidentified peaks were observed in the SAXS measurement of oral dry powder formulations (Fig. 3-3e-f).

The drug absorption from oral LC formulations was dramatically affected by the MGE concentration and the physicochemical properties of entrapped drugs (Fig. 3-4). The bioavailability of PABA was significantly improved by the 20% MGE formulation (OP20) compared with other LC formulations or PABA solution alone (Fig. 3-4a). These results indicated that the rate limiting step in the absorption of hydrophilic drugs must be the permeating process through the intestinal membrane. Thus, the hexosome particles in contact with the small intestine were high in this formulation (OP20) by increasing the MGE concentration.

In contrast, in case of M-PABA and E-PABA entrapping formulations, a low concentration of MGE (OM10 and OE10) significantly improved the bioavailability of PABA compared with other LC formulations or PABA solution alone (Fig. 3-4b and c). These results indicated that the rate limiting step in the absorption process of lipophilic drugs with LC formulations must be their release rate. Thus, the release amount of these drugs

increased from these formulation (OM10 and OE10) by decreasing the MGE concentration. This could be also the reason why the absorption of M-PABA and E-PABA from the LC formulations was delayed compared with PABA-LC formulation (Table 3-4). Furthermore, M-PABA and E-PABA were metabolized to PABA after oral administration of their LC formulations, indicating that LC systems were unable to protect these drugs from intestinal esterase metabolite activity

Dry powdered oral LC formulations did not manage to form hexosomes or cubosomes, which could be a reason why these formulations were unable to improve the bioavailability of PABA.

In consequence, as the same as in the *in vivo* oral absorption, *in vitro* skin permeation results were dramatically affected by the MGE concentration. Significant improvement in the skin penetration of Na-FL was observed in 20% and 30% MGE (TF20 and TF30) with enhancement ratios of 4.3 and 2.9, respectively. However, no marked improvement was observed in 10% and 40% MGE, suggesting that a low concentration of MGE such as 10% (TF10) could lead to a reduction in hexosomes particles. Thus, it is necessary to overcome the barrier function of stratum corneum. On the other hand, a high concentration of MGE such as 40% (TF40) reduced drug release from the formulation (Fig. 3-5).

The detailed mechanism of the enhanced oral drug absorption and transdermal drug penetration by LC systems is not fully understood yet [73, 77]. Further studies must be conducted to clarify the absorption-enhancing mechanism of LC formulations.

3.5. Chapter conclusion

The present data showed that LC formulations are promising to improve oral absorption and transdermal penetration of drugs. Our findings showed that the concentrations of LC-forming lipid and the physicochemical properties of entrapped drugs are very important factors that should be considered by researchers in this field to improve the performance of LC formulations in various pharmaceutical applications. Understanding the effect of these factors on the LC formulation performance could enable researchers to develop LC formulation approaches that intended to improve the oral absorption and skin permeation of drugs.

Conclusion

From all results obtained above, the following conclusion can be obtained:

1. Skin drug delivering using orally dispersed LC formulations could be a promising achievement in cosmeceutical, dietary and clinical fields. The drug plasma concentration can be modified based on the type and of LC forming lipid used in the formulation design.

2. The present results strongly suggested that the low viscosity of LC-formulations might influence drug diffusivity and permeability through skin. The present MGE-LC forming lipid can be utilized as a promising new topical formulation for therapeutic drugs and cosmetic ingredients. The recently developed MGE-LC-forming lipid can be utilized as a promising new topical formulation for therapeutic drugs and cosmetic ingredients.

3. The concentrations of LC-forming lipid and the physicochemical properties of entrapped drugs are very important factors that should be considered by researchers in this field to improve the performance of LC formulations in various pharmaceutical applications. Understanding the effect of these factors on the LC formulation performance could enable researchers to develop LC formulation approaches that intended to improve the oral absorption and skin permeation of drugs.

The findings of this study showed that LC formulations, such as cubosomes and hexosomes, represent an important class of biocompatible amphiphiles and their application can be extended to several fields, such as cosmeceutical, dietary and pharmaceutical technologies because of their remarkable structural complexity and usefulness in various pharmaceutical applications.

Acknowledgment

First of all, I would like to express my sincere gratitude to my supervisor Professor Kenji Sugibayashi (Laboratry of pharmaceutics and cosmeceutics, Faculty of Pharmaceutical Sciences, Josai University) for the continuous support of my Ph.D study, for his patience, motivation, and immense knowledge. His guidance helped me in all the time of research and writing of this thesis. Without his guidance and constant feedback this Ph.D would not have been achievable. I could never find enough words to truly express my gratitude to Professor Kenji Sugibayashi, withiout him I wouldn't be able to acheachive my dreams.

I would like to express my deepest gratitude to Acossiated Professor Hiroaki Todo for his invaluable advices and feedbacks on my research and for always being so supportive of my work. I appreciate all his contributions of time and ideas to make my Ph.D.

My sincere thanks also goes to Professor Konstanty Wierzba and Professor Tomomi Hatanaka for their kind support throughout my research.

Finally, I would like to express my deepest gratitude to my family. This dissertation would not have been possible without their warm love, continued patience, and endless support. I am indebted to my wife and her family for their love, understanding and especially making it possible for me to get a Ph.D degree in Japan. My wife, Mai, thank you for waiting with patience for last four years to become a complete family, without you it would not be possible to complete my study. To my life and soul, my son, thank you for being such a good little baby during my Ph.D study and making it possible for me to complete what I started. My family, wife and son are the most important people in my world and I dedicate this thesis to them.

References

1. Mark, R. P.; Robert, L. Transdermal drug delivery. *Nat. Biotechnol*. **11**, 1261-1268 (2008).
2. Singh, T. R.; Garland, M. J.; Cassidy, C. M.; Migalska, K.; Demir, Y. K.; Abdelghany, S.; Ryan, E.; Woolfson, A. D.; Donnelly, R. F. Microporation techniques for enhanced delivery of therapeutic agents. *Recent Pat. Drug Deliv. Formul*. **4**, 1-17 (2010).
3. Spicer, P. T.; Hayden, K. L. Novel process for producing cubic liquid crystalline nanoparticles (cubosomes). *Langmuir*. **17**, 5748-5756 (2001).
4. Yamada, K.; Yamashita, J.; Todo, H.; Miyamoto, K.; Hashimoto, S.; Tokudome, Y.; Hashimoto, F.; Sugibayashi, K. Preparation and evaluation of liquid-crystal formulations with skin-permeation-enhancing abilities for entrapped drugs. *J Oleo Sci*. **60**, 31-40 (2011).
5. Schneeweis, A.; Mueller-Goymann, C. C. *In vivo* and *in vitro* diclofenac sodium evaluation after rectal application of soft gelatin capsules enabling application induced transformation (AIT) into a semisolid system of liquid crystals (SSLC) for controlled release. *Pharm. Res*. **14**, 1726-1729 (1997).
6. Gin, D. L.; Pecinovsky, C. S.; Bara, J. E.; Kerr, L. Functional lyotropic liquid crystal materials. *Struct. Bond*. **128**, 181-222 (2008).
7. Makai, M.; Csanyi, E.; Nemeth, Z.; Palinkas, J.; Eros, I. Structure and drug release of lamellar liquid crystals containing glycerol. *Int. J. Pharm*. **256**, 95-107 (2003).
8. Guo, C.; Wang, J.; Cao, F.; Lee, R. J.; Zhai, G. Lyotropic liquid crystal systems in drug delivery. *Drug Discov. Today*. **15**, 1032-1040 (2010).
9. Siddig, M. A.; Radiman, S.; Muniandy, S. V.; Jan, L. S. Structure of cubic phases in ternary systems glucopone/water/hydrocarbon. *Colloids Surf A Physicochem Eng Asp*. **236**, 57-67 (2004).
10. Fong, W. K.; Hanley, T.; Boyd, B. J. Stimuli responsive liquid crystals provide 'on-demand' drug delivery *in vitro* and *in vivo*. *J. Control. Release*. **135**, 218-226 (2009).

11. Clogston, J.; Rathman, J.; Tomasko, D.; Walker, H.; Caffrey, M. Phase behavior of a monoacylglycerol: (myverol 18-99 K)/water system. *Chem. Phys. Lipids*. **107**, 191-220 (2000).
12. Kadhum, W. R.; Todo, H.; Sugibayashi, K. Skin permeation: Enhancing ability of liquid crystal formulations. In: Dragicevic-Curic N, Maibach H (eds.). Percutaneous penetration enhancers chemical methods in penetration enhancement: Drug manipulation strategies and vehicle effects. Springer-Verlag Berlin Heidelberg. pp. 243-253 (2015).
13. Drummond, C. J.; Fong, C. Surfactant self-assembly objects as novel drug delivery vehicles. *Curr. Opin. Colloid Interface Sci*. **4**, 449-456 (1999).
14. Shah, J. C.; Sadhale, Y.; Chilukuri, D. M. Cubic phase gels as drug delivery systems. *Adva. Drug Deliv. Rev*. **47**, 229-250 (2001).
15. Kaasgaard, T.; Drummond, C. J. Ordered 2-D and 3-D nanostructured amphiphile self-assembly materials stable in excess solvent. *Phys. Chem. Chem. Phys.* **8**, 4957-4975 (2006).
16. Chong, J. Y. T.; Mulet, X; Waddington, L. J.; Boyd, B. J.; Drummond, C. J. High-throughput discovery of novel steric stabilizers for cubic lyotropic liquid crystal nanoparticle dispersions. *Langmuir*. **28**, 9223-9232 (2012).
17. Spicer, P. T. Progress in liquid crystalline dispersions: cubosomes. *Curr Opin Colloid Interface Sci*. **10**, 274-279 (2005).
18. Yaghmur, A.; Glatter, O. Characterization and potential applications of nanostructured aqueous dispersions. *Adv. Colloid Interface Sci*. **148**, 333-342 (2009).
19. Lancelot, A.; Sierra, T.; Serrano, J. L. Nanostructured liquidcrystalline particles for drug delivery. *Expert Opin Drug Deliv*. **11**, 1-18 (2014).
20. Hirlekar, R.; Jain, S.; Patel, M.; Garse, H.; Kadam, V. Hexosomes: a novel drug delivery system. *Curr. Drug Deliv*. **7**, 28-35 (2010).
21. Sonja, S.; Nikola, G.; Robert, Z.; Wolfgang, S. Oxidation of ortho- and para-amino benzoic acid. A pulse radiolysis-and gamma radiolysis study. *Radiat. Phys. Chem*. **80**, 932-936 (2010).

22. Hu, M. L.; Chen, Y. K.; Chen, L. C.; Sano, M. Para-aminobenzoic acid scavenges reactive oxygen species and protects DNA against UV and free radical damage. *J Nutr Biochem*. **6**, 504-508 (1995).
23. Akberova, S. I. New biological properties of *p*-aminobenzoic acid. *Biol. Bull*. **29**, 390-393 (2002).
24. Rashmi, S. S.; Raechel, C. J.; Carol, J. B.; Mario, G. F.; Alexei, P. L.; Megan, A. M. Effects of *p*-aminobenzoic acid (PABA) form and administration mode on PABA recovery in 24-hour urine collections. *J. Acad. Nutr. Diet*. **114**, 458-463 (2013).
25. Zarafonetis, C. J.; Dabich, L.; Skovronski, J. J. Retrospective studies in scleroderma: skin response to potassium para-aminobenzoate therapy. *Clin. Exp. Rheumatol*. **6**, 261-268 (1988).
26. Zarafonetis, C. J.; Dabich, L.; Negri, D. Retrospective studies in scleroderma: effect of potassium para-aminobenzoate on survival. *J. Clin. Epidemiol*. **41**, 193-205 (1988).
27. Ichikawa, M.; Watanabe, S.; Miyake, Y. A new multiple-unit oral floating dosage system. II: *In vivo* evaluation of floating and sustained release characteristics with para amino benzoic acid and isosorbide dinitrate as model drugs. *J. Pharm. Sci*. **80**, 1153-1156 (1991).
28. Nguyen, T. H.; Hanley, T.; Porter, C. J.; Boyd, B. J. Nanostructured liquid crystalline particles provide long duration sustained-release effect for a poorly water soluble drug after oral administration. *J. Control. Release*. **153**: 180-186 (2011).
29. Higuchi, T. Mechanism of sustained action medication: theoretical analysis of rate of release of solid drugs dispersed in solid matrices. *J. Pharm. Sci*. **52**, 1145-1148 (1963).
30. Anderson, D. M.; Gruner, S. M.; Leibler, S. Geometrical aspects of the frustration in the cubic phases of lyotropic liquid crystals. *Proc. Natl. Acad. Sci. USA*. **85**, 5364-5368 (1988).
31. Qiu, H.; Caffrey, M. The phase diagram of monoolein/water system: metastability and equilibrium aspects. *Biomaterials*. **21**, 223-234 (2000).

32. Azmi, I. D.; Wu, L.; Wibroe, P. P.; Nilsson, C.; Østergaard, J.; Stürup, S.; Gammelgaard, B.; Urtti, A.; Moghimi, S. M.; Yaghmur, A. Modulatory effect of human plasma on the internal nanostructure and size characteristics of liquid-crystalline nanocarriers. *Langmuir*. **31**, 5042-5049 (2015).
33. Wibroe, P. P.; Azmi, I. D.; Nilsson, C.; Yaghmur, A.; Moghimi, S. M. Citrem modulates internal nanostructure of glyceryl monooleate dispersions and bypasses complement activation: Towards development of safe tunable intravenous lipid nanocarriers. *Nanomedicine*. **11**, 1909-1914 (2015).
34. Barauskas, J.; Cervin, C.; Jankunec, M.; Spandyreva, M.; Ribokaite, K.; Tiberg, F.; Johnsson, M. Interactions of lipid-based liquid crystalline nanoparticles with model and cell membranes. *Int. J. Pharm.* **391**, 284-291 (2010).
35. Murgia, S.; Falchi, A. M.; Mano, M.; Lampis, S.; Angius, R.; Carnerup, A. M.; Schmidt, J.; Diaz, G.; Giacca, M.; Talmon, Y.; Monduzzi, M. Nanoparticles from lipid-based liquid crystals: emulsifier influence on morphology and cytotoxicity. *J. Phys. Chem*. **114**, 3518-3521 (2010).
36. Shen, H. H.; Crowston, J. G.; Huber, F.; Saubern, S.; McLean, K. M.; Hartley, P. G. The influence of dipalmitoyl phosphatidylserine on phase behaviour of and cellular response to lyotropic liquid crystalline dispersions. *Biomaterials*. **31**, 9473-9481 (2010).
37. Ganem-Quintanar, A.; Quintanar-Guerrero, D. A review of the pharmaceutical applications. *Drug Dev. Ind. Pharm*. **26**, 809-820 (2000).
38. Ericsson, B.; Ericsson, P. O.; Lofroth, J. E.; Engstrom, S. Cubic phases as delivery systems for peptide drugs. *Am. Chem. Soc. Symp. Ser*. **469**, 251-265 (1991).
39. Boyle, E.; German, J. B. Monoglycerides in membrane systems. *Crit Rev Food Sci Nutr*. **36**, 785-805 (1996).
40. Longer, M.; Tyle, P.; Mauger, J. W. A cubic-phase oral drug delivery system for controlled release of AG337. *Drug Dev. Ind. Pharm.* **22**, 603-608 (1996).
41. Shen, H. H.; Crowston, J. G.; Huber, F.; Saubern, S.; McLean, K. M.; Hartley, P. G. The influence of dipalmitoyl phosphatidylserine on phase behaviour of and cellular response to lyotropic liquid crystalline dispersions. *Biomaterials*. **31**, 9473-9481 (2010).

42. Hinton, T. M.; Grusche, F.; Acharya, D.; Shukla, R.; Bansal, V.; Waddington, L. J.; Monaghan, P.; Muir, B. W. Bicontinuous cubic phase nanoparticle lipid chemistry affects toxicity in cultured cells. *J. Toxicol. Res*. **3**, 11-22 (2014).
43. Barauskas, J.; Landh, T. Phase behaviour of the phytantriol/water system. *Langmuir*. **19**, 9562-9565 (2003).
44. Briggs, J.; Chung, H.; Caffrey, M. The temperature-composition phase diagram and mesophase structure characterization of the monoolein/water system. *J Phys II France*. **6**, 723-751 (1996).
45. Kathy, W. Y. L.; Nguyen, T. H.; Hanley, T.; Boyd, B. J. Nanostructure of liquid crystalline matrix determines *in vitro* sustained release and *in vivo* oral absorption kinetics for hydrophilic model drugs. *Int. J. Pharm*. **365**, 190-199 (2009).
46. Bu, M.; Tang, J.; Wei, Y.; Sun, Y.; Wang, X.; Wu, L.; Liu, H. Enhanced bioavailability of nerve growth factor with phytantriol lipid-based crystalline nanoparticles in cochlea. *Int. J. Nanomed*. **10**, 6879-6889 (2015).
47. Yaghmur, A.; Rappolt, M.; Østergaard, J.; Larsen, C.; Larsen, S. W. Characterization of bupivacaine-loaded formulations based on liquid crystalline phases and microemulsions: the effect of lipid composition. *Langmuir*. **28**, 2881-2889 (2012).
48. Boyd, B. J. Characterisation of drug release from cubosomes using the pressure ultrafiltration method. *Int. J. Pharm*. **260**, 239-47 (2003).
49. Larsson, K. Colloidal dispersions of ordered lipid-water phases. *J Dispersion Sci Technol*. **20**, 27-34 (1999).
50. Purdon, C. H.; Azzi, C. G.; Zhang, J.; Smith, E. W.; Maibach, H. I. Penetration enhancement of transdermal delivery-current permutations and limitations. *Crit. Rev. Ther. Drug Carrier Syst*. **21**, 97-132 (2004).
51. Kasha, P. C.; Banga, A. K. A review of patent literature for iontophoretic delivery and devices. *Recent Pat. Drug Deliv. Formul*. **2**, 41-50 (2008).
52. Ogura, M.; Paliwal, S.; Mitragotri S. Low-frequency sonophoresis: current status and future prospects. *Adv. Drug Deliv. Rev*. **60**, 1218-1223 (2008).

53. Tokumoto, S.; Mori, K.; Higo, N.; Sugibayashi, K. Effect of electroporation on the electroosmosis across hairless mouse skin *in vitro*. *J. Control. Release*. **105**, 296-304. (2005).
54. Tokudome, Y.; Sugibayashi, K. Mechanism of the synergic effects of calcium chloride and electroporation on the *in vitro* enhanced skin permeation of drugs. *J. Control. Release*. **95**, 267-274 (2004).
55. Larsson, K. Aqueous dispersions of cubic lipid–water phases. *Curr. Opin. Colloid.* **5**, 64-69 (2000).
56. Caboi, F.; Amico, G. S.; Pitzalis, P.; Monduzzi, M.; Nylander, T.; Larsson, K. Addition of hydrophilic and lipophilic compounds of biological relevance to the monoolein/water system. I. Phase behavior. *Chem. Phys. Lipids*. **109**, 47-62 (2001).
57. Dae, G. L.; Won, W. J.; Nam, A. K.; Jun, Y. L.; Seol, H. L.; Woo, S. S.; Nae, G. K.;Seong, H. J. Effect of the glyceryl monooleate-based lyotropic phases on skin permeation using *in vitro* diffusion and skin imaging. *Asian J. Pharm. Sci.* **9**, 324-329 (2014).
58. Chen Y, Ma P, Gui S. Cubic and hexagonal liquid crystals as drug delivery systems. *Biomed. Res. Int*. 2014, 2014, 1.
59. Biltonen, R. L.; Lichtenberg, D. The use of differential scanning calorimetry as a tool to characterize liposome preparations. *Chem. Phys. Lipids*. **64**, 128-42 (1993).
60. Bode, J. C.; Kuntsche, J.; Funari, S. S.; Bunjes, H. Interaction of dispersed cubic phases with blood components. *Int. J. Pharm*. **448**, 87-95 (2013).
61. Kadhum, W. R.; Oshizaka, T.; Hijikuro, I.; Todo, H.; Sugibayashi, K. Usefulness of liquid–crystal oral formulations to enhance the bioavailability and skin tissue targeting of *p*-amino benzoic acid as a model compound. *Eur. J. Pharm. Sci*. **88**, 282-290 (2016).
62. Wallin, R.; Engstrom, S.; Mandenius, C. F. Stabilisation of glucose oxidase by entrapment in a cubic liquid crystalline phase. *Biocatalysis*. **8**, 73–80 (1993).
63. Nylander, T.; Mattisson, C.; Razumas, V.; Miezes, Y.; Hakansson, B. A study of entrapped enzyme stability and substrate diffusion in a monoglyceride-based cubic liquid crystalline phase. *Colloids Surf. A*. **114**, 311-320 (1996).

64. Caboi, F.; Nylander, T.; Razumas, V.; Talaikyte, Z.; Monduzzi, M.; Larsson, K. Structural effects, mobility, and redox behavior of vitamin K1 hosted in the monoolein:water liquid crystalline phases. *Langmuir*. **13**, 5476-5483 (1997).
65. Lopes, L. B.; Speretta, F. F.; Bentley, M. Enhancement of skin penetration of vitamin K using monoolein-based liquid crystalline systems. *Eur. J. Pharm. Sci*. **32**, 209-215 (2007).
66. Wong, J.; Abrishami, A.; El Beheiry, H.; Mahomed, N. N.; Roderick D. J.; Gandhi, R.; Syed K. A.; Muhammad O. H. S.; De Silva, Y.; Chung, F. Topical application of tranexamic acid reduces postoperative blood loss in total knee arthroplasty: a randomized, controlled trial. *J. Bone Joint Surg. Am*. **15**, 2503-2513 (2010).
67. Wada, Y.; Ishii, F. Potential Power of Green Tea Catechins. *J. Oleo Sci*. **8**, 371-378 (2008).
68. Siekmann, B.; Bunjes, H.; Koch, M. H. J.; Westesen, K. Preparation and structural investigations of colloidal dispersions prepared from cubic monoglyceride water phases. *Int. J. Pharm*. **244**, 33-43 (2002).
69. Esposito, E.; Eblovi, N.; Rasi, S.; Drechsler, M.; Di Gregorio, G.; Menegatti, E.; Cortesi, R. Lipid-based supramolecular systems for topical application: a preformulatory study. *AAPS PharmSciTech*. **5**, 1-15 (2003).
70. Sherif, S.; Bendas, E. R.; Badawy, S. The clinical efficacy of cosmeceutical application of liquid crystalline nanostructured dispersions of alpha lipoic acid as anti-wrinkle. *Eur. J. Pharm. Biopharm*. **86**, 251–259 (2014).
71. Watanabe, T.; Hasegawa, T.; Takahashi, H.; Ishibashi, T.; Takayama, K.; Sugibayshi, K. Utility of the three-dimensional cultured human skin model as a tool to evaluate skin permeation of drugs. *AATEX*. **8**, 1-14 (2001).
72. Morimoto, Y.; Hatanaka, T.; Sugibayashi, K.; Omiya, H. Prediction of skin permeability of drugs: comparison of human and hairless rat skin. *J. Pharm. Pharmacol*. **44**, 634-639 (1992).
73. Uchino, T.; Murata, A.; Miyazaki, Y.; Oka, T.; Kagawa, Y. Glyceryl monooleyl ether-based liquid crystalline nanoparticles as a transdermal delivery system of flurbiprofen: characterization and *in vitro* transport. *Chem. Pharm. Bull*. **63**, 334-340 (2015).

74. Esposito, E.; Cortesi, R.; Drechsler, M.; Paccamiccio, L.; Mariani, P.; Contado, C.; Stellin, E.; Menegatti, E.; Bonina, F.; Puglia, C. Cubosome dispersions as delivery systems for percutaneous administration of indomethacin. *Pharm. Res*. **22**, 2163-2173 (2005).
75. Evenbratt, H.; Jonsson, C.; Faergemann, J.; Engstrom, S.; Ericson, M. B. In vivo study of an instantly formed lipid–water cubic phase formulation for efficient topical delivery of aminolevulinic acid and methyl-aminolevulinate. *Int. J. Pharm.* **452**, 270-275 (2013).
76. Lopes, L. B.; Ferreira, D. A.; de Paula, D.; Garcia, M. T.; Thomazini, J. A.; Fantini, M. C.; Bentley, M. V. Reverse hexagonal phase nanodispersion of monoolein and oleic acid for topical delivery of peptides: *in vitro* and *in vivo* skin penetration of cyclosporin A. *Pharm. Res*. **23**, 1332-1342 (2006).
77. Okawara, M.; Hashimoto, F.; Todo, H.; Sugibayashi, K.; Tokudome, Y. Effect of liquid crystals with cyclodextrin on the bioavailability of a poorly water-soluble compound, diosgenin, after its oral administration to rats. *Int. J. Pharm*. **472**, 257–261 (2014).
78. Ali, A.; Kataoka, N.; Ranneh, A.; Iwao, Y.; Noguchi, S.; Oka, T.; Itai, S. Enhancing the solubility and oral bioavailability of poorly water-soluble drugs using monoolein cubosomes. *Chem. Pharm. Bull*. **65**, 42-48 (2017).
79. Cohen-Avrahami, M.; Aserin, A.; Garti, N. HII mesophase and peptide cell-penetrating enhancers for improved transdermal delivery of sodium diclofenac. *Colloids Surf. B Biointerfaces*. **77**, 131-138 (2010).
80. Weiss, V. M.; Naolou, T.; Hause, G.; Kuntsche, J.; Kressler, J.; Mader, I. Poly (glycerol adipate)-fatty acid esters as versatile nanocarriers: from nanocubes over ellipsoids to nanospheres, *J. Control. Release*. **158**, 156‑164 (2012).

Appendix

Supplementary data

Fig. 2-2

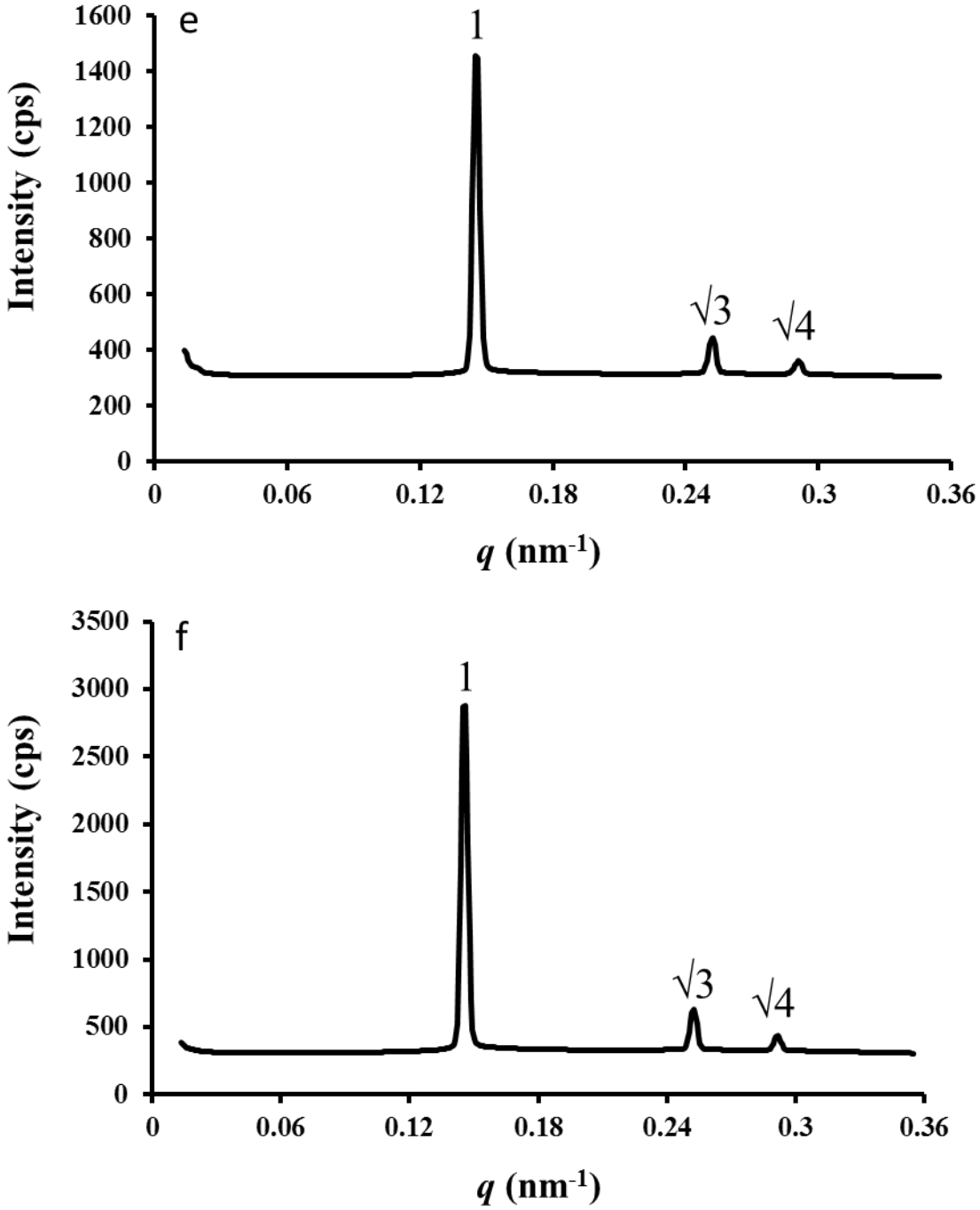

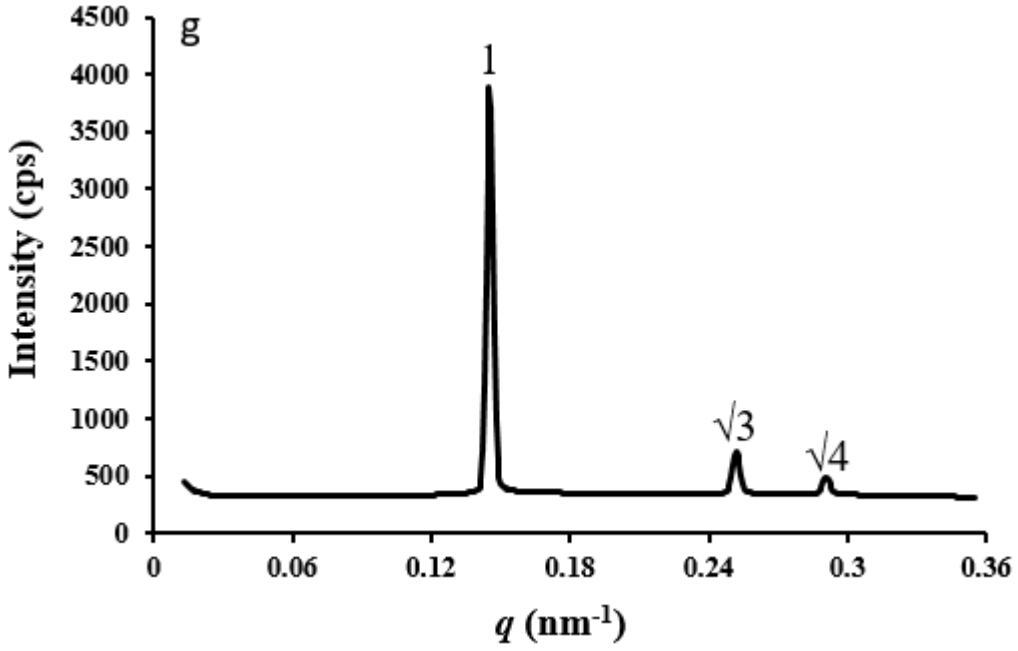
g
1
√3
√4
Intensity (cps)
4500
4000
3500
3000
2500
2000
1500
1000
500
0
0
0.06
0.12
0.18
0.24
0.3
0.36
q (nm-1)

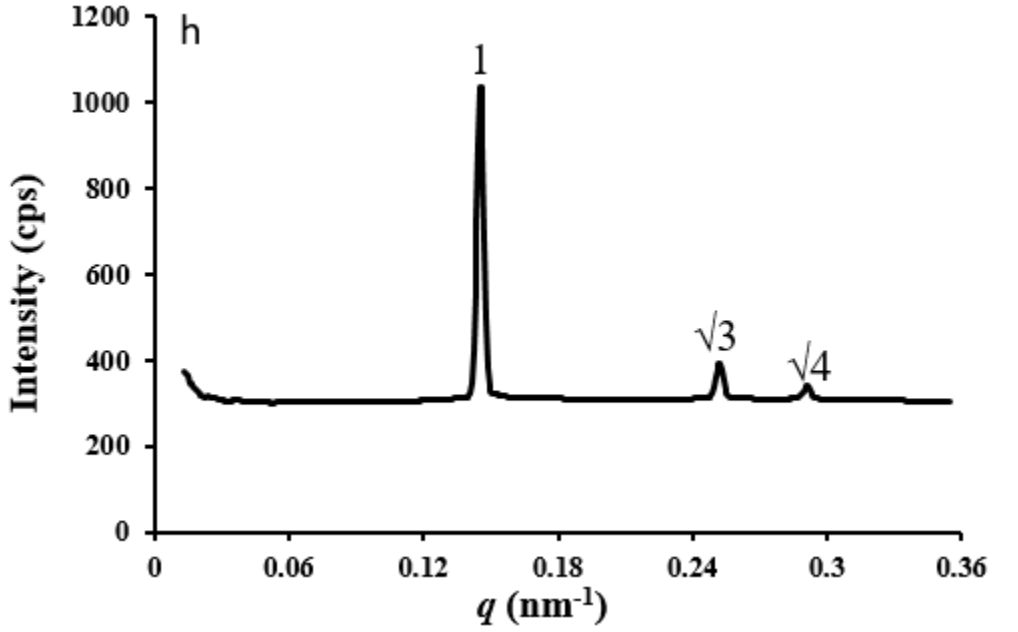
h
1
√3
√4
Intensity (cps)
1200
1000
800
600
400
200
0
0
0.06
0.12
0.18
0.24
0.3
0.36
q (nm-1)

Fig. 2-3

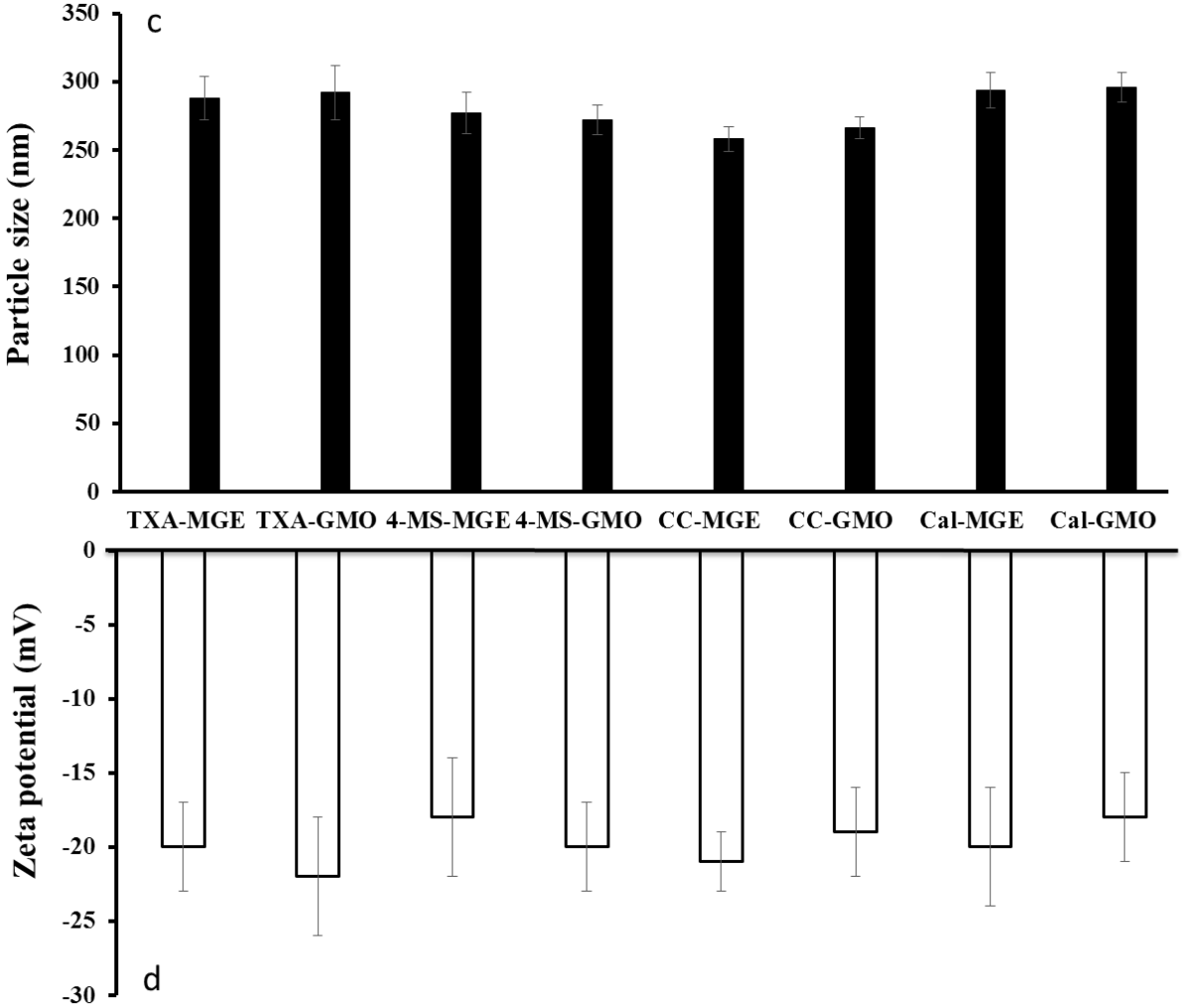
c
Particle size (nm)
350
300
250
200
150
100
50
0
TXA-MGE
TXA-GMO
4-MS-MGE
4-MS-GMO
CC-MGE
CC-GMO
Cal-MGE
Cal-GMO
0
-5
-10
-15
-20
-25
-30
Zeta potential (mV)
d